Geoscience Frontiers xxx (2016) 1–25

HOSTED BY

ELSEVIER

Contents lists available at ScienceDirect

China University of Geosciences (Beijing)

Geoscience Frontiers

journal homepage: www.elsevier.com/locate/gsf

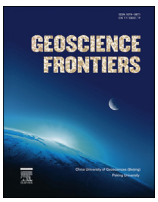

Research paper

Petrogenesis of Quebrada de la Mina and Altar North porphyries (Cordillera of San Juan, Argentina): Crustal assimilation and metallogenic implications

Laura Maydagán [a,b,*], Marta Franchini [a,c,d], Massimo Chiaradia [e], Verónica Bouhier [a,b], Noelia Di Giuseppe [a,d], Roger Rey [f], Luis Dimieri [b]

[a] Centro Patagónico de Estudios Metalogenéticos-CONICET, Argentina
[b] INGEOSUR-CONICET, Departamento de Geología, Universidad Nacional del Sur, San Juan 670, 8000 Bahía Blanca, Argentina
[c] Instituto de Investigación en Paleobiología y Geología, Universidad Nacional de Río Negro, Av. Roca 1242, 8332 Roca, Argentina
[d] Departamento de Geología y Petróleo, Facultad de Ingeniería, Universidad Nacional del Comahue, Buenos Aires 1400, 8300 Neuquén, Argentina
[e] Section of Earth and Environmental Sciences, University of Geneva, Switzerland
[f] Minera Peregrine Argentina S.A, Santa Fe (Oeste) 117, Piso 4B, Edificio Derby, Ciudad San Juan, Argentina

ARTICLE INFO

Article history:
Received 13 January 2016
Received in revised form
25 October 2016
Accepted 24 November 2016
Available online xxx
Handling Editor: W. Xiao

Keywords:
Porphyry
High sulfidation epithermal
Magmatic recharge
Radiogenic isotopes
Crustal assimilation
Argentinian Andes

ABSTRACT

We investigate the geology of Altar North (Cu–Au) and Quebrada de la Mina (Au) porphyry deposits located in San Juan Province (Argentina), close to the large Altar porphyry copper deposit (995 Mt, 0.35% Cu, 0.083 g/t Au), to present constraints on the magmatic processes that occurred in the parental magma chambers of these magmatic-hydrothermal systems. Altar North deposit comprises a plagioclase-amphibole-phyric dacite intrusion (Altar North barren porphyry) and a plagioclase-amphibole-biotite-phyric dacite stock (Altar North mineralized porphyry, 11.98 ± 0.19 Ma). In Quebrada de la Mina, a plagioclase-amphibole-biotite-quartz-phyric dacite stock (QDM porphyry, 11.91 ± 0.33 Ma) crops out. High Sr/Y ratios (92–142) and amphibole compositions of Altar North barren and QDM porphyries reflect high magmatic oxidation states (fO_2 = NNO +1.1 to +1.6) and high fH_2O conditions in their magmas. Zones and rims enriched in anorthite (An_{37-48}), SrO (0.22–0.33 wt.%) and FeO (0.21–0.37 wt.%) in plagioclase phenocrysts are evidences of magmatic recharge processes in the magma chambers. Altar North and Quebrada de la Mina intrusions have relatively homogeneous isotopic compositions ($^{87}Sr/^{86}Sr_{(t)}$ = 0.70450–0.70466, $\varepsilon_{Nd}(t)$ = +0.2 to +1.2) consistent with mixed mantle and crust contributions in their magmas. Higher Pb isotopes ratios ($^{207}Pb/^{204}Pb$ = 15.6276–15.6294) of these intrusions compared to other porphyries of the district, reflect an increase in the assimilation of high radiogenic Pb components in the magmas. Ages of zircon xenocrysts (297, 210, 204, 69 Ma) revealed that the magmas have experienced assimilation of Miocene, Cretaceous, Triassic and Carboniferous crustal rocks.

Fluids that precipitated sulfides in the Altar deposit may have remobilized Pb from the host rocks, as indicated by the ore minerals being more radiogenic ($^{207}Pb/^{204}Pb$ = 15.6243–15.6269) than their host intrusions. Au/Cu ratio in Altar porphyries (average Au/Cu ratio of 0.14×10^{-4} by weight in Altar Central) is higher than in the giant Miocene porphyry deposits located to the south: Los Pelambres, Río Blanco and Los Bronces (Chile) and Pachón (Argentina). We suggest that the increase in Au content in the porphyries of this region could be linked to the assimilation of high radiogenic Pb components in the magmas within these long-lived maturation systems.

1. Introduction

Porphyry Cu–Au–Mo deposits can be developed over time spans that may last up to several million years (Sillitoe, 2010). During this period magmas and parental plutons associated

* Corresponding author. Centro Patagónico de Estudios Metalogenéticos-CONICET, Argentina.
E-mail address: lauramaydagan@yahoo.com.ar (L. Maydagán).
Peer-review under responsibility of China University of Geosciences (Beijing).

http://dx.doi.org/10.1016/j.gsf.2016.11.011

with the porphyries may experience processes such as recharge, mixing and assimilation of crustal rocks (e.g. Keith et al., 1997; Hattori and Keith, 2001; Maughan et al., 2002; Halter et al., 2004, 2005; Cooke et al., 2005; Audétat and Pettke, 2006; Chiaradia et al., 2009, 2012; Sun et al., 2015) that may influence the metal budget and evolution of the magmatic-hydrothermal system. However, little is known about the link between these magmatic processes and the formation of large copper deposits.

The Altar porphyry Cu–(Au) (31°29′S, 70°30′W) is a large Cu and Au deposit (measured and indicated resources of 2057 Mt @ 0.332% Cu and 0.79 g/t Au, Marek, 2014) located in the SW of San Juan Province, Argentina (Fig. 1). Sparse outcrops in this area obscure the volcanic stratigraphy and intrusive relationships, making more difficult the task of understanding the geology. Maydagán et al. (2011) presented the first geological map of the Altar region, as well as petrographic, geochemical, isotopic (Sr, Nd, Pb) analyses, and LA-ICP-MS geochronology of the Miocene igneous rocks of the area. A late Carboniferous tonalitic batholith occurs on the east side of the Altar district (Fig. 2; Maydagán, 2012) and Cretaceous sedimentary rocks are present along the Argentinian-Chilean boundary, to the west (Mpodozis et al., 2009). The Altar district is hosted by early Miocene volcanic rocks (Maydagán et al., 2011) which are equivalent to the Abanico Formation in Chile (Klohn, 1960), the Pachón Formation in the vicinity of the Los Pelambres deposit, the Coya Machalí Formation in the El Teniente area (Charrier et al., 2002) and the Doña Ana Group of the El Indio belt (Kay and Mpodozis, 2002; Winocur et al., 2014). Early Miocene volcanic rocks consist of an intercalation of basaltic andesite and porphyritic andesite-dacite lavas, levels of andesitic-dacitic lapilli tuff, and pyroclastic breccia that grade upwards to an upper unit of compacted and thick rhyolitic tuff (Maydagán et al., 2011). The volcanic sequence is deformed by folding and faulting and was intruded by middle to late Miocene porphyritic andesite-dacite dikes, stocks and breccias (Maydagán et al., 2011). Altar is a complex magmatic-hydrothermal system characterized by the superposition of several magmatic and hydrothermal pulses (Maydagán et al., 2011; Maydagán et al., 2014). The Au/Cu ratio of 0.14×10^{-4} by weight across Altar central ridge is low compared with the Cu–Au porphyries of the Andean back-arc region, but higher than the Au/Cu ratio of the giant nearby porphyry deposits Los Pelambres, El Pachon, Río Blanco, and Los Bronces (Zwahlen et al., 2014). Plagioclase phenocrysts from Altar porphyries suggest a process of magmatic recharge by less evolved magmas in shallow magmatic chambers (Maydagán et al., 2014).

Recently, two new Cu–Au prospects were discovered near Altar: Quebrada de la Mina (QDM, Au) and Altar North (AN, Cu–Au; Figs. 2 and 3). The objective of this work is to extend and deepen the geological knowledge of this important mining district located in the Argentinian Andes with huge metallogenic potential but still little geological knowledge. To accomplish this task, we investigate the geology of these two new prospects, QDM and AN. This work presents the first field mapping, petrographic and geochemical analyses of these areas, coupled with analyses of mineral chemistry (amphibole, biotite, plagioclase), new laser ablation-inductively coupled plasma-mass spectrometry (LA-ICP-MS) U–Pb dating, and isotopic (Sr, Nd, Pb) data of intrusions and mineralization. Elemental analyses across plagioclase crystals were carried out to elucidate processes occurring in the magma chambers. Finally, we relate these new areas chronologically and genetically with Altar (Central and

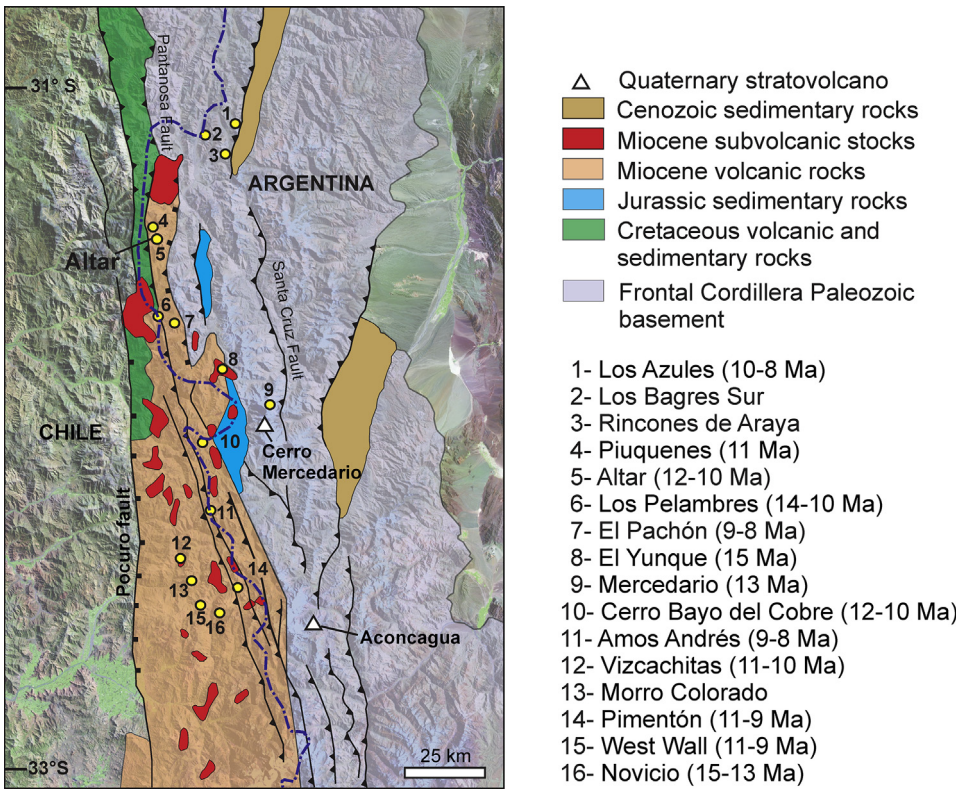

Figure 1. Geologic map of the Miocene intra-arc basin showing the location and ages of the Miocene–Pliocene porphyry copper deposits of Chile and Argentina (Mpodozis and Cornejo, 2012, and references therein).

Please cite this article in press as: Maydagán, L., et al., Petrogenesis of Quebrada de la Mina and Altar North porphyries (Cordillera of San Juan, Argentina): Crustal assimilation and metallogenic implications, Geoscience Frontiers (2016), http://dx.doi.org/10.1016/j.gsf.2016.11.011

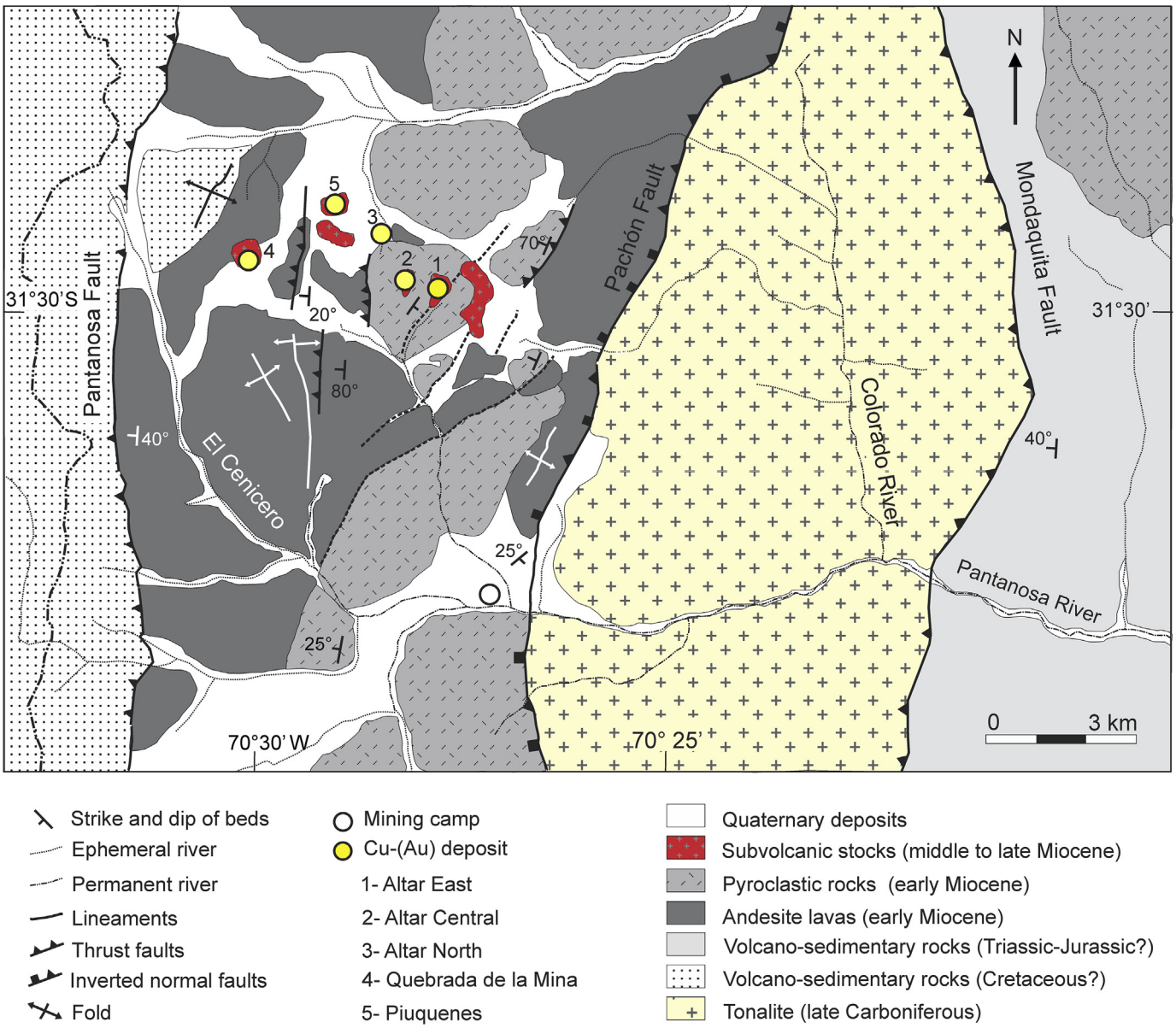

Figure 2. Geologic map of the Altar region showing the location of Cu–(Au) deposits and regional faults.

East; Fig. 3) and integrate the data into a possible petrogenetic model of the Altar mining district.

2. Regional geological setting

The Altar region is located in the Andean Main Cordillera over the inactive volcanic flat-slab segment (28°–33°S) of the Southern Central Andes (Fig. 1). In this region of South America, the Nazca plate is subducting nearly horizontally beneath the South American plate at ~100 km depth (Cahill and Isacks, 1992; Anderson et al., 2007; Gans et al., 2011).

From 35 to 21 Ma, in the western part of the Cordillera Principal between 32°S and 37°S, thick volcano-sedimentary sequences accumulated under an extensional tectonic regime (Charrier et al., 2002) in volcano-tectonic depressions or intra-arc basins (Abanico basin in the study area; Muñoz et al., 2006; Mpodozis and Cornejo, 2012, Fig. 1). These sequences were assigned to the Abanico, Coya-Machalí, and Cura-Mallín formations (e.g. Jordan et al., 2001; Charrier et al., 2002; Kay and Mpodozis, 2002; Farías et al., 2008). During Oligocene times a magmatic intra-arc basin occupied the axial part of the main Andes between 29°S and 30°S under an extensional tectonic regime (Winocur and Ramos, 2008). This intra-arc basin is represented by the Doña Ana Group, composed of the Tilito and Escabroso formations, and the retro-arc is occupied by the Valle del Cura and Río La Sal formations (Winocur et al., 2014).

During the early Miocene (27–20 Ma), this segment had a subducted slab geometry similar to that currently observed in the normal-slab segment at 35°S, and a crustal thickness of 35–40 km (Kay and Mpodozis, 2002). The shallowing of the subduction zone progressed from middle to late Miocene (20–5 Ma), accompanied by the subduction of the Juan Fernández ridge (e.g. Yáñez et al.,

Please cite this article in press as: Maydagán, L., et al., Petrogenesis of Quebrada de la Mina and Altar North porphyries (Cordillera of San Juan, Argentina): Crustal assimilation and metallogenic implications, Geoscience Frontiers (2016), http://dx.doi.org/10.1016/j.gsf.2016.11.011

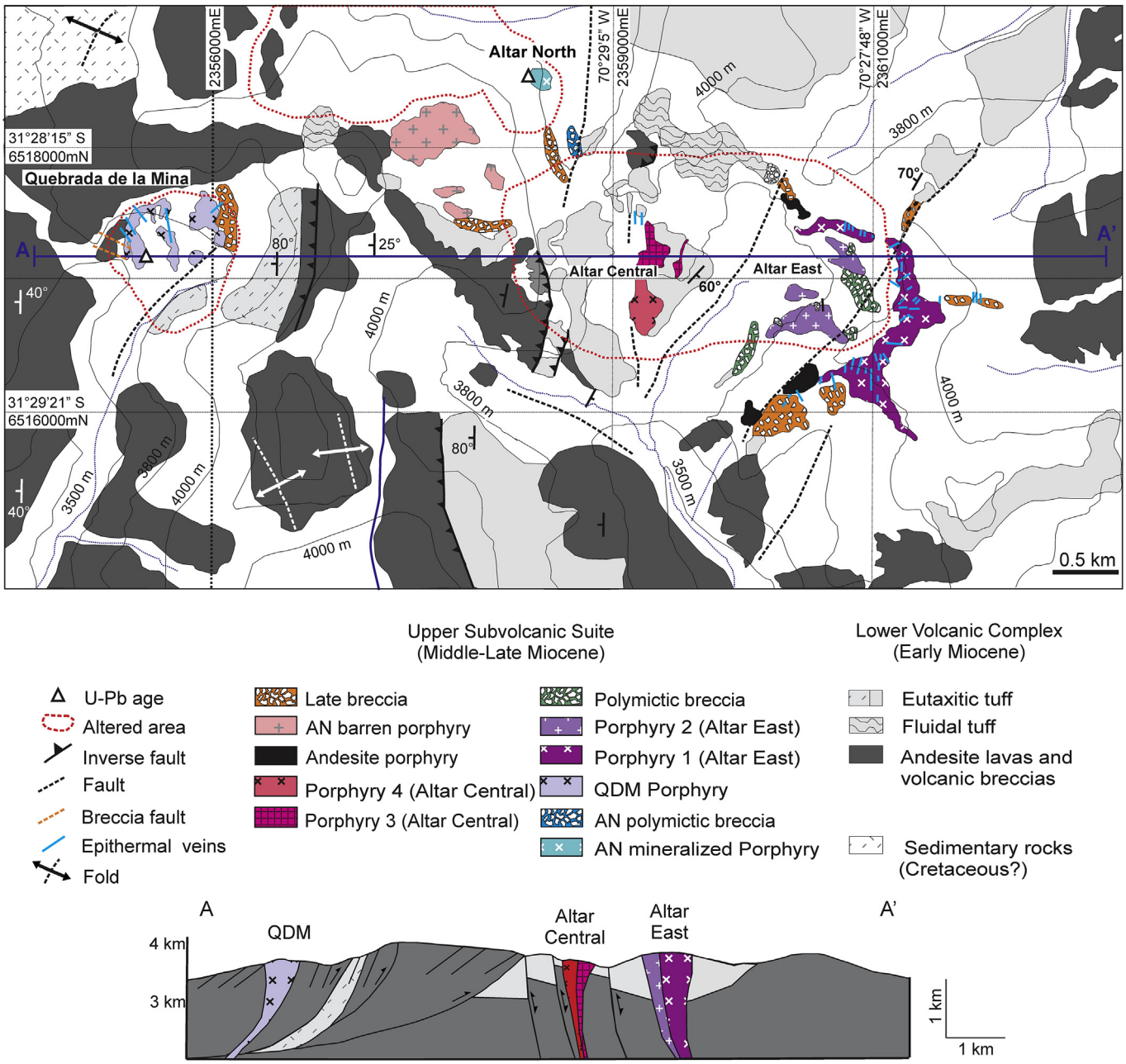

Figure 3. Detailed map of the study area including lithologic units, major structures (faults and bedding), rivers, altered area, and location of structural section A–A′.

2001) and eastward migration and broadening of the arc (Kay and Mpodozis, 2002).

The basin of the early Miocene volcanic rocks hosts numerous Cu (Au–Mo) deposits linked to late Miocene porphyritic intrusions (15 to 8 Ma, Mpodozis and Cornejo, 2012, Fig. 1). The emplacement of the porphyries took place under a compressive regime and crustal shortening. Basin inversion and significant tectonic uplift of the Principal Andean Cordillera occurred as a result of the Neogene compressive tectonism (Maksaev et al., 2009). Cessation of the magmatic activity over the flat-slab Miocene arc occurred at 5 Ma. Subsequent magmatism over the flat-slab occurred in the back-arc, in particular the Farallón Negro, Pocho, and San Luis magmatic centers (Kay and Mpodozis, 2002).

3. Local geology

3.1. Geological mapping

We have expanded the mapped area of Maydagán et al. (2011) covering the new mineralized prospects (Figs. 2 and 3). A structural section was compiled considering information from the surface and subsurface of the area (Fig. 3).

3.1.1. Altar North area

The AN prospect area is mostly covered by rock debris with very few outcrops (Figs. 3 and 4a). Early Miocene lava flows and pyroclastic rocks of the lower volcanic complex crop out on the eastern

Please cite this article in press as: Maydagán, L., et al., Petrogenesis of Quebrada de la Mina and Altar North porphyries (Cordillera of San Juan, Argentina): Crustal assimilation and metallogenic implications, Geoscience Frontiers (2016), http://dx.doi.org/10.1016/j.gsf.2016.11.011

ridges of this area (Maydagán et al., 2011). The N–S lineament of AN valley suggests the presence of a fault system at depth (Figs. 3 and 4a).

Two porphyry intrusions were distinguished in the AN prospect based on their texture and abundance of phenocrysts. A dacite stock (AN barren porphyry) is exposed on the western ridges at elevations of ~4000 m.a.s.l (Figs. 3 and 4a). The porphyritic texture is defined by two populations of phenocrysts of plagioclase (55 vol.%, 0.1 to 0.3 mm and 1 to 4 mm) and amphibole (5–8 vol.%; 0.1 to 0.2 mm and 1 to 3 mm), scarce quartz phenocrysts, and accessory apatite (0.05 mm) set in a microcrystalline (0.02–0.05 mm) quartz + feldspar groundmass (Fig. 4b). It is fresh or affected by weak propylitic alteration and is barren. Locally, this intrusion is affected by silicification and intense argillic alteration.

A porphyritic stock (AN mineralized porphyry) crops out in this area (Figs. 3 and 4a). This stock contains phenocrysts of plagioclase (55%, 1–3 mm), biotite (1%, 1–5 mm) and amphibole (1%, 1–3 mm) set in a fine-grained groundmass (Fig. 4c). This porphyry differs from the other porphyries due to the finer grained size of the phenocrysts. AN mineralized porphyry has undergone phyllic, propylitic and supergene alterations, is crosscut by a stockwork of quartz veins (up to 25 vol.%), and is overprinted by Cu–Au mineralization (Fig. 4d). Small outcrops of a polymictic, matrix to clast-supported breccia with fragments of porphyritic stocks and tuff (up to 2 cm in diameter) surrounded by a mud-sized matrix occur in the central Altar North valley (AN polymictic breccia, Fig. 4e). This breccia has been affected by intense phyllic alteration. A polymictic matrix-supported breccia (Late Breccia, mapped previously at Altar East, Maydagán et al., 2014) crops out in the Altar North valley (Figs. 3 and 4f). The breccia contains subangular to angular fragments (0.2 mm–4 cm) of volcanic rocks and porphyritic intrusions in a fine-grained matrix and has been affected by phyllic and supergene alteration. This breccia is widespread in the Altar district, located at the contacts of the porphyries with the wall-rocks. In some places it is stratified and in others it has a chaotic arrangement with clasts showing a great variety of grain sizes.

3.1.2. Quebrada de la Mina area

North of QDM prospect, an intercalation of red sandstones and conglomerates affected by folding are exposed (Fig. 2). The age of these rocks is estimated to be Cretaceous to early Miocene (Mpodozis, personal communication). The early Miocene lower volcanic complex is widespread at QDM (Figs. 3 and 5a, b) and consists of intercalations of basaltic andesite lavas, porphyritic andesite lavas, and polymictic volcanic breccias that grade upwards to levels dominated by pyroclastic rocks (Fig. 5c, d). The volcanic sequence is affected by deformation and on the western ridges shows a N–S trend and dips ~40° to the west (Figs. 3 and 5a, b). The pyroclastic rocks can be classified as eutaxitic (Fig. 5c) and rheomorphic tuffs (Fig. 5d; Branney and Kokelaar, 2002). The eutaxitic tuffs have a lower proportion of quartz phenocrysts compared to the Altar rhyolitic tuffs (Maydagán et al., 2011). The rheomorphic tuffs crop out on the north and eastern ridges of QDM (Fig. 5b). Early Miocene volcanic rocks were intruded by a circular dacite porphyry stock, approximately 0.6 km in diameter (QDM porphyry), that crops out on the northern ridges of the prospect (Fig. 5b). QDM porphyry has phenocrysts of plagioclase (35–40 vol.%, 0.1–7 mm), amphibole (5 vol.%, 0.2–2 mm), biotite (1.5 vol.%, 5 mm), quartz (1.5–3 vol.%, 0.2–2 mm) in a microgranular (0.01–0.02 mm) to submicroscopic groundmass. Unlike other Altar porphyries, QDM porphyry is distinguished by its larger phenocrysts of quartz, plagioclase and biotite, which are strongly fractured (Fig. 5e). QDM porphyry underwent appreciable gold introduction associated with sericitic and tourmaline + pyrite (±quartz ± sericite) alterations. To the east, the QDM porphyry presents a porphyritic facies with phenocrysts of plagioclase (45 vol.%, 0.2–3 mm) and biotite (3 vol.% 0.2–1 mm) in a submicroscopic groundmass, and lacks quartz and amphibole phenocrysts. A polymictic matrix-supported breccia (Late Breccia) with a N–S trend intruded the volcanic sequence and the QDM porphyry. It contains rounded fragments of porphyry, volcanic rocks and breccias (up to 60 cm) in a mud-sized greenish matrix (Fig. 5f). Locally, monomictic clast-supported tourmaline-cemented breccias cut the volcanic rocks, the porphyry, and the matrix supported breccia (Fig. 5g).

4. Analytical techniques and sampling methodology

Forty five days were spent mapping during field campaigns in 2013–2015. Mapping of 150 structural data (bedding dip and orientation) of faults, fault-breccias, veins, and joints was also compiled. A selection of 12 drill cores from QDM and AN was inspected. Lithology, contact relationships, alteration assemblages, and veining were described and 80 samples were collected.

Polished thin sections ($n = 41$) from AN and QDM samples were examined using a Nikon petrographic microscope to document the mineralogy and alteration assemblages.

Two samples corresponding to QDM porphyry (drill hole QDM–21, 209/212 m depth) and AN porphyry (drill hole ALD–160, 246/250 m depth) were selected for LA-ICP-MS U–Pb dating in zircons (Table 1, Digital Appendices A and B). Samples were analyzed in the laboratory of geochronology of the British Columbia University (Canada). Zircons were analyzed using LA-ICP-MS, employing methods described by Tafti et al. (2009). Instrumentation comprises a New Wave UP–213 laser ablation system and a Thermo Finnigan Element2 single collector, double-focusing, magnetic sector ICP-MS. Analytical methods are described in the Digital Appendix D to this paper.

Fresh samples ($n = 7$) from QDM and AN prospects were selected for major and trace element analysis. Major, trace and rare earth elements were analyzed by ICP emission spectrometry and ICP mass spectrometry (Group 4A–4B combined package) at Acme Analytical Laboratories Ltd., Canada (Table 2).

Chemical compositions of plagioclase ($n = 98$), amphibole ($n = 8$), and biotite ($n = 10$) were determined with a JEOL JXA 8230 electron microprobe at the LAMARX laboratories, Universidad Nacional de Córdoba (Argentina), equipped with two wavelength dispersive spectrometers (WDS) and one energy dispersive spectrometer (EDS). Operating conditions were 15 kV and 30 nA with a beam diameter of 5 μm. The standards, analytical lines and limits of detection (wt.%) were as follows: F (topaz, K_α, 0.02), Na (anorthoclase, K_α, 0.01), Mg (forsterite, K_α, 0.01), Al (anorthoclase, K_α, 0.01), Si(rhodonite, K_α, 0.01), Cl (sodalite, K_α, 0.01), K (orthoclase, K_α, 0.01), Ca (wollastonite, K_α, 0.01), Ti (TiO_2, K_α, 0.01), Mn (rhodonite, K_α, 0.02), Fe (fayalite, K_α, 0.02), Sr (celestine, L, 0.03). The full data set of the microprobe analysis is provided in Tables 3–5.

Four samples were analyzed for Sr and Nd isotopes and six for Pb isotopes at the Department of Earth Sciences, University of Geneva (Switzerland) following the method of Chiaradia et al. (2009; Table 6).

5. Results

5.1. Geochronology

Twenty spot analyses on zircon crystals from the fine-grained AN mineralized porphyry defined a weighted mean $^{206}Pb/^{238}U$

Please cite this article in press as: Maydagán, L., et al., Petrogenesis of Quebrada de la Mina and Altar North porphyries (Cordillera of San Juan, Argentina): Crustal assimilation and metallogenic implications, Geoscience Frontiers (2016), http://dx.doi.org/10.1016/j.gsf.2016.11.011

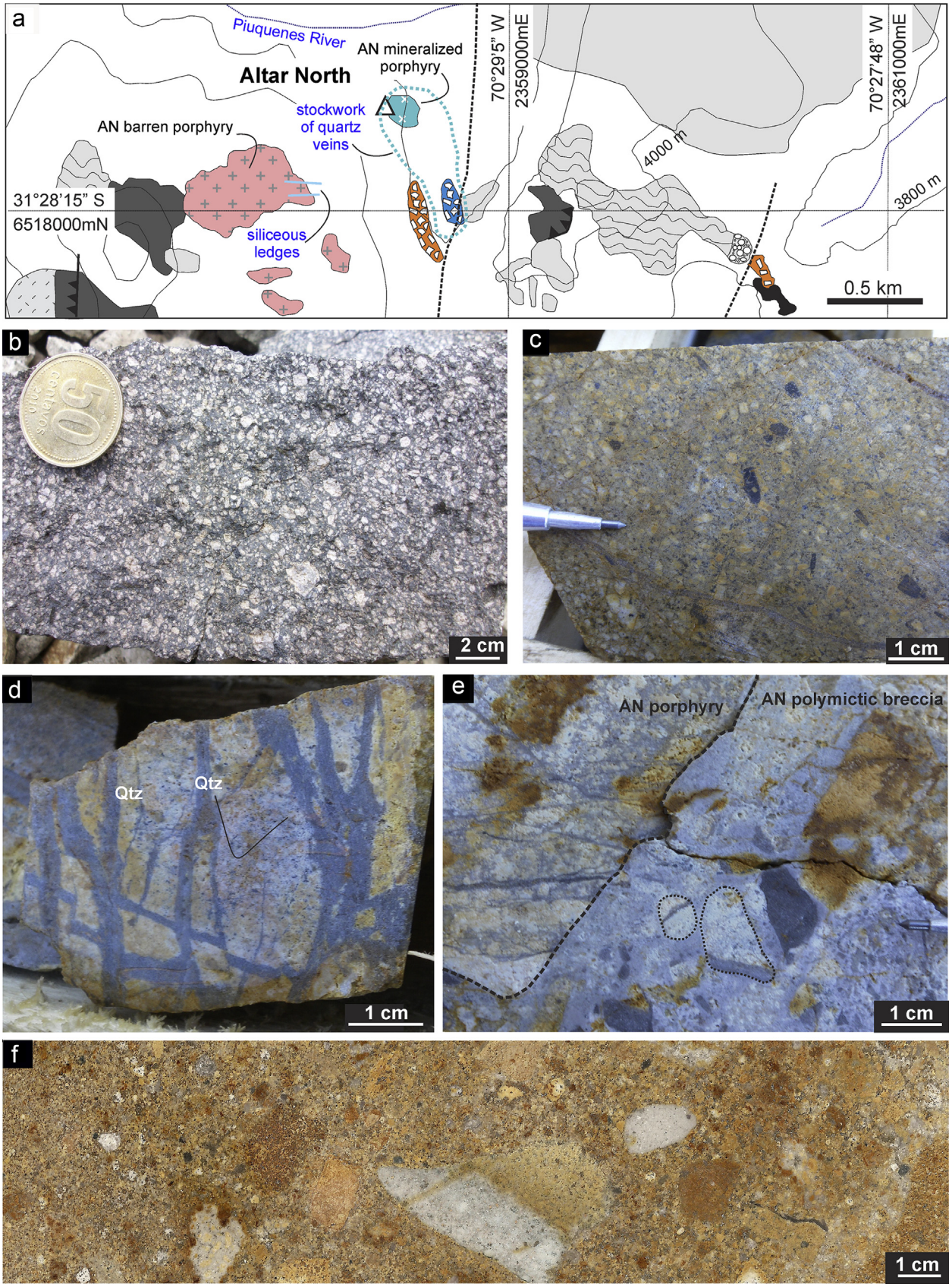

Figure 4. (a) Geologic map of Altar North deposit; (b) AN barren stock characterized by two populations of plagioclase and hornblende phenocrysts; (c) AN mineralized porphyry intercepted in the drill hole ALD–160; (d) quartz veins cutting the AN mineralized stock; (e) AN polymictic breccia cut the AN mineralized porphyry; (f) polymictic matrix-supported breccia (Late Breccia) with rounded fragments of porphyritic rocks, affected by supergene alteration.

Please cite this article in press as: Maydagán, L., et al., Petrogenesis of Quebrada de la Mina and Altar North porphyries (Cordillera of San Juan, Argentina): Crustal assimilation and metallogenic implications, Geoscience Frontiers (2016), http://dx.doi.org/10.1016/j.gsf.2016.11.011

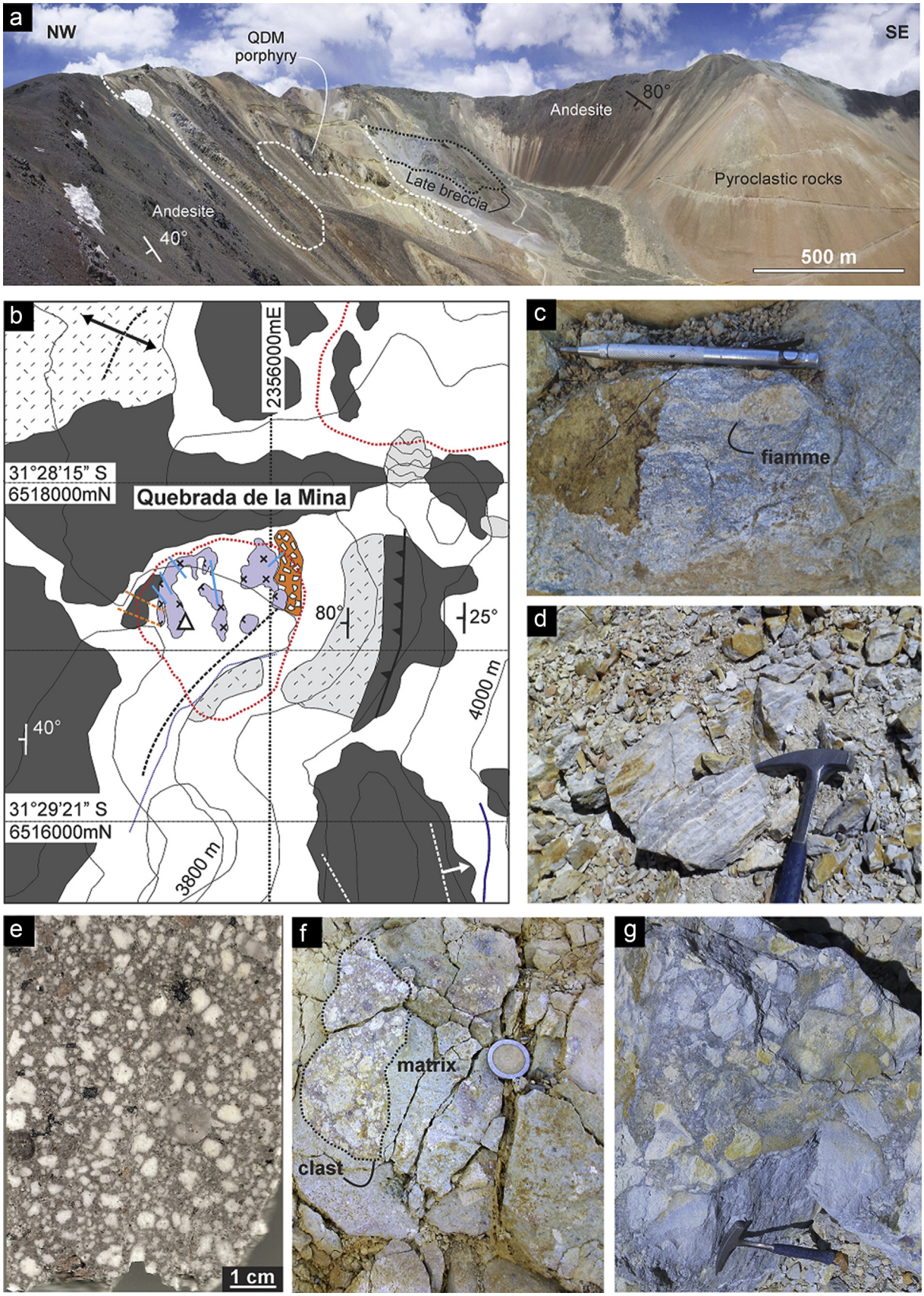

Figure 5. (a) View of QDM deposit looking to the north; (b) geologic map of QDM deposit; (c) exposures of eutaxitic tuff at QDM; (d) fluidal tuff; (e) QDM porphyry with phenocrysts of plagioclase, amphibole, biotite, and quartz in a microgranular groundmass; (f) polymictic matrix-supported breccia (Late Breccia) with fragments of breccia in a mud-sized greenish matrix; (g) monomictic clast-supported hydrothermal tourmaline-cemented breccia (very small outcrops, not included in Fig. 3).

Please cite this article in press as: Maydagán, L., et al., Petrogenesis of Quebrada de la Mina and Altar North porphyries (Cordillera of San Juan, Argentina): Crustal assimilation and metallogenic implications, Geoscience Frontiers (2016), http://dx.doi.org/10.1016/j.gsf.2016.11.011

Table 1
U–Pb LA-ICP-MS dating in zircons.

Sample no	Intrusion	Easting[a]	Northing[a]	Elevation (m)	Analyses	Age (Ma)	2σ ±	MSWD
QDM-21	Quebrada de la Mina porphyry	23,55,700	65,17,700	3670	18	11.91	0.33	1.9
ALD-160	Altar North mineralized porphyry	23,58,600	65,18,400	3612	20	11.98	0.19	0.83

[a] The sample location coordinates are provided in Gauss Krueger, Inchauspe (2, Fig. 3).

age of 11.98 ± 0.19 Ma, with MSDW of 0.83 and a probability of 0.68 (Fig. 6), which is interpreted to be the crystallization age of the subvolcanic stock.

Eighteen spot zircon analyses of the porphyritic facies of QDM porphyry yielded a mean crystallization $^{206}Pb/^{238}U$ age of 11.91 ± 0.33 Ma, with a MSDW of 1.9 and a probability of 0.016 (Fig. 7). One older zircon with an age of 69.3 ± 1.85 Ma was not included in the age calculation.

5.2. Geochemistry

5.2.1. Major, trace, rare earth elements and mineral chemistry

The chemical analyses of igneous rocks are presented in Table 2 together with the location and estimated intensity of alteration of each sample. The AN mineralized porphyry was not analyzed due to its strong hydrothermal alteration. In the total alkali versus silica diagram (Fig. 8a), samples from the AN barren and the QDM intrusions plot close to the boundary of dacite (granodiorite) and trachyte (syenite) fields and are subalkaline. We have assessed the element mobility in the samples in order to evaluate the effects of hydrothermal alteration. In the Zr/TiO_2 versus Nb/Y diagram (modified from Winchester and Floyd, 1977; Wu et al., 2015; Fig. 8b), most samples from AN and QDM porphyries plot on the boundary between trachy andesite (monzonite) and andesite (diorite). The samples analyzed lack hydrothermal quartz addition, thus the differences observed in Fig. 8b could be explained by the very low Y values (3.6–9 ppm) of these intrusions. In the diagram SiO_2 versus Zr/TiO_2 (Winchester and Floyd, 1977), AN and QDM porphyries plot in the boundary between andesite (diorite) and dacite (granodiorite) fields, similar to the Altar Central porphyries (Fig. 8c). In the K_2O versus SiO_2 diagram, the freshest samples of QDM and AN barren dacite intrusions plot close to the boundary between low and medium K fields (Fig. 8d). Two samples from the QDM intrusion show higher K_2O values (2.7–3.1 wt.%, Table 2), coinciding with samples that have the plagioclase partially altered to potassium feldspar and illite. These diagrams show that although there has been some potassium enrichment in some of the samples, most of the major and trace elements have remained unaffected. In the Na_2O versus SiO_2 plot (Fig. 8e), the samples show less scatter (3.9–5.6 wt.%) as is the case for the other major elements. TiO_2 displays relatively tight trends (0.6–0.8 wt.%) when plotted against SiO_2 (Fig. 8f). The AN barren porphyry has a SiO_2 range from 63.2 to 63.5 wt.% and QDM intrusion ranges between 63.1 and 64.3 wt.% (Fig. 9a). Fe_2O_3 contents range between 2.9 and 3.7 wt.% in QDM porphyry, and between 3.5 and 3.7 wt.% in the AN barren porphyry (Fig. 9b). Altar North barren and QDM porphyries have high Sr/Y ratios (92–142). The La/Sm, Sm/Yb and Sr/Y ratios of QDM porphyry and AN barren porphyry versus time are shown in Fig. 9c–e. Bulk rock REE analyses of QDM and AN barren porphyries normalized to chondrite abundances (Boynton, 1989) define patterns with a pronounced negative slope (Fig. 9f) and no Eu anomalies.

Representative major element compositions of plagioclase crystals are presented in Table 3. Plagioclase from QDM porphyry has a lower range of anorthite compositions ($An_{11–39}$) than plagioclase from the AN barren porphyry ($An_{23–48}$, Table 3).

In the AN barren porphyry, most of the analyzed plagioclase phenocrysts have oscillatory compositional zoning with zones of oligoclase ($An_{24–28}$) alternating with zones of andesine ($An_{37–39}$) (Fig. 10a). The increase in the anorthite molar content in the outer edge of the phenocrysts (An_{38}) is accompanied by an increase in FeO (0.23 wt.%) and SrO (0.23 wt.%, Fig. 10a). Other phenocrysts show a core and mantle with homogeneous oligoclase composition ($An_{26–27}$) and an outer edge enriched in anorthite ($An_{41–48}$), FeO (0.32–0.37 wt.%), and SrO (0.22–0.25 wt.% (Fig. 10b). Fig. 10c shows the content of FeO (wt.%) versus the molar content of anorthite in plagioclase from AN barren porphyry.

Most large phenocrysts of plagioclase from QDM porphyry are fractured and show oscillatory zoning with alternating zones of andesine ($An_{30–49}$) and oligoclase ($An_{25–29}$). Some phenocrysts have oligoclase cores ($An_{25–30}$) and zones with increase in anorthite content ($An_{30–38}$), that do not match with significant changes in FeO or SrO. However, small phenocrysts show oligoclase cores ($An_{22–26}$) and an outer edge enriched in anorthite ($An_{30–38}$), FeO (0.21 wt.%), and SrO (0.22 wt.%, Fig. 11a). Other phenocrysts have cores of oligoclase surrounded by bands of andesite and oligoclase and an outer rim enriched in anorthite ($An_{30–38}$) and SrO (0.19 wt.%, Fig. 11b). Fig. 11c shows the contents of FeO (wt.%) versus the molar content of anorthite in plagioclase from QDM porphyry. Anorthite values lower than An_{10} in QDM porphyry are indicative of hydrothermal alteration of the plagioclase to K feldspar or albite (Digital Appendix C).

Plagioclase from Altar North and QDM have excess of aluminum ($(Al/(Ca + Na + K)–1)/0.01An) > 1$) plotting in the fertile field of Williamson et al., 2016 (Fig. 11d). Amphibole from AN barren porphyry corresponds to edenite according to the classification of Leake et al. (1997, Table 4). Biotites from QDM plot in the calc-alkaline field of Abdel Rahman (1994, Table 5).

5.3. Sr–Nd–Pb isotopes

New isotopic data for barren and mineralized AN and QDM intrusions and for sulfides of the mineralization are reported in Table 6. The analyzed sulfides (pyrite and galena) belong to late veinlets of the Altar deposit (E veins) considered epithermal or transitional to an epithermal environment.

The subvolcanic intrusions have relatively homogeneous isotopic compositions ($^{87}Sr/^{86}Sr_{(t)}$ = 0.70450–0.70466, $\varepsilon_{Nd}(t)$ = +0.2 to +1.2, $^{206}Pb/^{204}Pb$ = 18.6087–18.6200, $^{207}Pb/^{204}Pb$ = 15.6276–15.6294, $^{208}Pb/^{204}Pb$ = 38.5472–38.5623 (Fig. 12). Fig. 12a, b show the new isotope data of the ore minerals, and AN and QDM intrusions, together with data of Altar volcanic and subvolcanic rocks previously obtained by Maydagán et al. (2011, 2014). Most samples from the AN and the QDM porphyries plot in the mantle array (Fig. 12a). They have slightly lower $^{87}Sr/^{86}Sr$ ratios than the porphyries from Altar East and Altar Central (Fig. 12b). Samples from the AN barren and QDM porphyries, and Altar ore minerals plot in a trend cutting the orogene curve of Zindler and Hart (1986, Fig. 12b). Altar ore

Please cite this article in press as: Maydagán, L., et al., Petrogenesis of Quebrada de la Mina and Altar North porphyries (Cordillera of San Juan, Argentina): Crustal assimilation and metallogenic implications, Geoscience Frontiers (2016), http://dx.doi.org/10.1016/j.gsf.2016.11.011

Table 2
Representative chemical analyzes of QDM, Altar North, Altar Central and Altar East porphyries.

Lithology	Tuff	Porphyry	Porphyry	Porphyry	Porphyry	Dacite stock	Dacite stock
Deposit	QDM	QDM	QDM	QDM	QDM	Altar North	Altar North
Sample	A314	A1014	A1014 bis	QDM-21-200	QDM-21-202	A-13-13	A-154-08
wt.%							
SiO_2	64.69	64.12	64.25	63.82	63.16	63.26	63.55
Al_2O_3	18.66	18.62	18.54	16.74	17.69	17.94	17.84
Fe_2O_3	3.10	3.53	3.64	3.79	2.93	3.75	3.54
MgO	0.62	1.20	1.28	1.35	1.54	1.41	1.38
CaO	0.32	2.20	2.17	1.50	0.99	3.60	4.22
Na_2O	3.49	5.28	5.45	5.00	3.99	5.65	5.47
K_2O	2.31	1.61	1.54	2.72	3.13	1.63	1.80
TiO_2	0.99	0.69	0.69	0.58	0.57	0.67	0.66
P_2O_5	0.11	0.08	0.07	0.18	0.23	0.23	0.24
MnO	0.02	0.03	0.03	0.60	0.14	0.09	0.05
Cr_2O_3	0.01	0.00	<0,002	<0,002	<0,002	<0,002	<0,002
LOI	5.50	2.40	2.10	3.30	4.60	1.5	1.00
Sum	99.85	99.76	99.77	99.56	99.01	99.76	99.75
ppm							
Ni	35.00	<20	<20	<20	<20	<20	3.10
Sc	17	4	4	4	4	6	4
Ba	432	484	421	797	887	552	561
Be	2.00	2.00	1.00	<1	<1	<1	2.00
Co	1.40	4.80	4.60	7.00	5.80	6.7	7.60
Cs	33.80	55.00	53.70	6.20	9.90	1.5	1.50
Ga	18.90	25.70	23.50	21.20	21.10	24.2	24.0
Hf	5.70	4.00	3.60	3.00	2.90	3.4	3.60
Nb	9.80	4.80	4.60	4.50	4.40	4.8	5.40
Rb	45.90	59.90	58.80	44.90	59.30	35.7	43.50
Sn	3.00	2.00	2.00	<1	<1	<1	1.00
Sr	182.40	837.40	799.70	522.10	468.40	905.4	1019.50
Ta	0.70	0.30	0.30	0.40	0.40	0.3	0.40
Th	4.90	3.30	3.00	3.10	3.10	3.0	3.30
U	1.60	1.00	1.00	1.20	1.40	1.1	1.10
V	101	73	75	62	65	82	77
W	1.60	<0,5	<0,5	<0,5	<0,5	<0,5	0.70
Zr	213.30	147.60	135.90	104.90	100.30	127.2	141.30
Y	30.00	9.10	6.70	5.00	3.60	7.9	7.20
La	21.60	21.50	21.60	11.90	14.50	19.6	19.50
Ce	48.70	45.20	44.50	26.80	35.50	41.9	42.20
Pr	6.16	5.40	5.28	3.41	4.39	5.22	5.49
Nd	27.20	21.10	20.50	13.70	15.90	21.1	22.30
Sm	6.28	3.45	2.93	2.42	2.46	3.51	3.53
Eu	1.53	0.89	0.86	0.72	0.74	0.98	0.99
Gd	5.70	2.30	1.98	1.63	1.59	2.42	2.25
Tb	0.90	0.30	0.26	0.20	0.19	0.31	0.28
Dy	5.13	1.54	1.28	1.07	0.86	1.55	1.28
Ho	1.12	0.24	0.23	0.16	0.14	0.27	0.23
Er	3.23	0.72	0.66	0.50	0.40	0.72	0.59
Tm	0.51	0.11	0.09	0.07	0.06	0.10	0.08
Yb	3.35	0.67	0.66	0.51	0.41	0.67	0.58
Lu	0.50	0.09	0.08	0.08	0.08	0.10	0.09
Mo	1.00	1.30	1.40	0.20	0.20	0.9	0.40
Cu	25.20	52.20	53.90	8.30	103.50	17.3	28.20
Pb	6.70	20.30	19.40	9.30	13.90	8.0	1.40
Zn	32	101	104	2027	6331	136	47
Ni	0.80	3.50	3.50	5.50	3.80	4.2	<20
As	49.10	38.80	32.70	40.60	45.90	16.5	14.70
Cd	0.10	0.10	<0,1	1.60	14.40	0.2	<0,1
Sb	1.90	7.70	6.00	0.40	0.30	0.5	0.10
Bi	<0,1	<0,1	0.10	0.40	0.40	<0,1	<0,1
Ag	<0,1	0.10	0.10	0.70	1.80	<0,1	<0,1
Au	4.10	9.00	5.00	19.20	41.80	<0,5	<0,5
Hg	<0,01	<0,01	<0,01	<0,01	0.01	0.04	0.04
Tl	0.30	0.50	0.50	<0,1	<0,1	<0,1	<0,1
Se	0.60	<0,5	<0,5	<0,5	0.70	<0,5	<0,5
Easting[a]	23,55,780	23,56,018	23,56,018	23,55,717	23,55,717	23,57,939	23,57,906
Northing[a]	65,16,806	65,17,585	65,17,585	65,17,699	65,17,699	65,17,446	65,17,484
Int, Alt	Moderate	Fresh	Fresh	Weak	Weak	Fresh	Fresh

Int, Alt: Intensity of alteration, Weak: most plagioclase phenocrysts fresh, some mafic minerals preserved, texture intact; Moderate: plagioclase preserved, mafic minerals replaced, texture preserved; Strong: plagioclase altered, mafic minerals replaced, partial to total destruction of texture.
Notes: Major element, trace element analyses, and FeO were determined by inductively coupled mass spectroscopy, coupled plasma emission spectroscopy (ICP-ES), (ICP-MS) and dichromate titration, respectively, in ACME Analytical Laboratories Ltd, Vancouver, Canada.
[a] Locations are given in Gauss Krueguer coordinates, Inchauspe (2, Fig. 3).

Please cite this article in press as: Maydagán, L., et al., Petrogenesis of Quebrada de la Mina and Altar North porphyries (Cordillera of San Juan, Argentina): Crustal assimilation and metallogenic implications, Geoscience Frontiers (2016), http://dx.doi.org/10.1016/j.gsf.2016.11.011

Table 3
Representative electron microprobe analyses of plagioclase from QDM and Altar North porphyritic plutons.

Intrusion	Altar North porphyry																QDM porphyry																
Sample	A1313-C3									A156-C2							A1014-C3								A1014-C4								
Analysis	1	2	3	4	5	6	7	8	9	10	11	12	13	14	15	16	17	18	19	20	21	22	23	24	25	26	27	28	29	30	31	32	33
SiO_2	61.33	61.13	60.53	61.43	62.10	58.22	62.42	61.58	58.70	60.89	61.13	61.09	60.97	57.46	60.60	55.95	61.61	61.50	61.74	61.19	62.19	59.09	61.87	58.24	61.28	59.46	59.74	59.44	60.83	61.24	59.40	60.21	58.05
TiO_2	0.00	0.00	0.00	0.01	0.00	0.08	0.01	0.03	0.01	0.02	0.00	0.00	0.00	0.00	0.02	0.04	0.00	0.01	0.00	0.03	0.02	0.03	0.00	0.02	0.00	0.00	0.02	0.01	0.04	0.00	0.02	0.01	0.00
Al_2O_3	25.13	24.79	25.49	24.81	24.33	26.92	24.13	24.52	26.95	24.55	24.49	25.06	24.86	26.93	25.20	28.62	24.67	24.71	24.44	24.91	24.18	25.42	24.65	27.44	24.82	25.92	26.14	25.94	24.57	24.89	25.18	25.42	26.72
FeO	0.15	0.12	0.18	0.19	0.17	0.18	0.19	0.16	0.23	0.19	0.14	0.18	0.17	0.32	0.20	0.37	0.16	0.16	0.12	0.20	0.19	0.22	0.18	0.21	0.11	0.19	0.15	0.15	0.13	0.16	0.16	0.16	0.16
MnO	0.00	0.02	0.02	0.01	0.01	0.00	0.03	0.00	0.01	0.00	0.00	0.00	0.07	0.04	0.01	0.03	0.00	0.04	0.01	0.00	0.04	0.02	0.02	0.00	0.02	0.03	0.00	0.00	0.02	0.00	0.00	0.00	0.04
MgO	0.02	0.02	0.00	0.02	0.00	0.00	0.00	0.01	0.00	0.02	0.00	0.01	0.01	0.01	0.00	0.01	0.00	0.00	0.00	0.03	0.00	0.00	0.00	0.01	0.00	0.00	0.00	0.01	0.00	0.00	0.00	0.00	0.00
CaO	5.69	5.69	6.29	5.55	4.88	7.92	4.82	5.20	7.58	5.49	5.22	5.61	5.42	8.27	5.98	9.68	5.22	5.32	5.05	5.51	4.76	6.33	5.13	7.95	5.51	6.76	6.78	7.07	5.23	5.64	6.13	6.28	7.78
SrO	0.09	0.18	0.17	0.19	0.17	0.17	0.17	0.19	0.23	0.16	0.09	0.10	0.13	0.22	0.19	0.25	0.17	0.15	0.10	0.14	0.16	0.33	0.16	0.22	0.15	0.18	0.14	0.15	0.19	0.15	0.26	0.11	0.19
Na_2O	7.79	7.92	7.70	7.88	8.22	6.66	8.26	8.10	6.89	7.81	7.83	7.98	8.04	6.29	7.65	5.62	8.24	8.05	8.37	8.02	8.51	7.66	8.14	6.83	7.87	7.55	7.41	7.29	8.10	7.99	7.71	7.55	6.89
K_2O	0.53	0.49	0.47	0.50	0.54	0.30	0.51	0.52	0.34	0.53	0.47	0.46	0.49	0.31	0.45	0.14	0.47	0.45	0.49	0.41	0.47	0.33	0.47	0.26	0.48	0.38	0.37	0.36	0.50	0.48	0.42	0.41	0.34
Total	100.7	100.3	100.8	100.6	100.4	100.4	100.5	100.3	100.9	99.6	99.3	100.5	100.2	99.8	100.3	100.7	100.5	100.4	100.3	100.4	100.5	99.4	100.6	101.2	100.2	100.5	100.7	100.4	99.6	100.5	99.3	100.1	100.1
Structural formula calculated based on 8 oxygen atoms																																	
Si^{4+}	2.71	2.71	2.68	2.72	2.75	2.60	2.76	2.60	2.60	2.72	2.74	2.71	2.71	2.59	2.70	2.51	2.72	2.73	2.73	2.71	2.75	2.65	2.74	2.58	2.72	2.64	2.65	2.64	2.72	2.71	2.67	2.68	2.59
Ti^{4+}	0.00	0.00	0.00	0.00	0.00	0.00	0.00	0.00	0.00	0.00	0.00	0.00	0.00	0.00	0.00	0.00	0.00	0.00	0.00	0.00	0.00	0.00	0.00	0.00	0.00	0.00	0.00	0.00	0.00	0.00	0.00	0.00	0.00
Al^{3+}	1.31	1.30	1.33	1.30	1.27	1.42	1.26	1.41	1.41	1.29	1.29	1.30	1.30	1.43	1.32	1.51	1.29	1.29	1.27	1.30	1.26	1.34	1.29	1.43	1.30	1.36	1.37	1.36	1.29	1.30	1.33	1.33	1.41
Fe^{3+}	0.00	0.00	0.00	0.00	0.00	0.00	0.00	0.00	0.00	0.00	0.00	0.00	0.00	0.00	0.00	0.00	0.00	0.00	0.00	0.00	0.00	0.00	0.00	0.00	0.00	0.00	0.00	0.00	0.00	0.00	0.00	0.00	0.00
Fe^{2+}	0.01	0.00	0.01	0.01	0.01	0.01	0.01	0.01	0.01	0.01	0.01	0.01	0.01	0.01	0.01	0.01	0.01	0.01	0.00	0.01	0.01	0.01	0.01	0.01	0.00	0.01	0.01	0.01	0.00	0.01	0.01	0.01	0.01
Mn^{2+}	0.00	0.00	0.00	0.00	0.00	0.00	0.00	0.00	0.00	0.00	0.00	0.00	0.00	0.00	0.00	0.00	0.00	0.00	0.00	0.00	0.00	0.00	0.00	0.00	0.00	0.00	0.00	0.00	0.00	0.00	0.00	0.00	0.00
Mg^{2+}	0.00	0.00	0.00	0.00	0.00	0.00	0.00	0.00	0.00	0.00	0.00	0.00	0.00	0.00	0.00	0.00	0.00	0.00	0.00	0.00	0.00	0.00	0.00	0.00	0.00	0.00	0.00	0.00	0.00	0.00	0.00	0.00	0.00
Ca^{2+}	0.27	0.27	0.30	0.26	0.23	0.38	0.23	0.36	0.36	0.26	0.25	0.26	0.26	0.40	0.28	0.46	0.25	0.25	0.24	0.26	0.23	0.30	0.24	0.38	0.26	0.32	0.32	0.34	0.25	0.27	0.29	0.30	0.37
Sr	0.00	0.00	0.00	0.00	0.00	0.00	0.00	0.00	0.00	0.00	0.00	0.00	0.00	0.00	0.00	0.00	0.00	0.00	0.00	0.00	0.00	0.01	0.00	0.00	0.00	0.00	0.00	0.00	0.00	0.00	0.00	0.00	0.00
Na^{+}	0.67	0.68	0.66	0.68	0.71	0.58	0.71	0.59	0.59	0.68	0.68	0.69	0.69	0.55	0.66	0.49	0.71	0.69	0.72	0.69	0.73	0.67	0.70	0.59	0.68	0.65	0.64	0.63	0.70	0.69	0.67	0.65	0.60
K^{+}	0.03	0.03	0.03	0.03	0.03	0.02	0.03	0.02	0.02	0.03	0.03	0.03	0.03	0.02	0.03	0.01	0.03	0.03	0.03	0.02	0.03	0.02	0.03	0.01	0.03	0.02	0.02	0.02	0.03	0.03	0.02	0.02	0.02
Al^{*}	1.35	1.32	1.35	1.34	1.31	1.46	1.30	1.45	1.45	1.33	1.35	1.33	1.33	1.48	1.36	1.57	1.31	1.33	1.29	1.34	1.28	1.36	1.33	1.46	1.34	1.37	1.39	1.38	1.32	1.33	1.35	1.37	1.42
Or	3.11	2.83	2.69	2.90	3.16	1.72	2.96	3.00	1.99	3.08	2.78	2.63	2.83	1.84	2.60	0.83	2.70	2.60	0.25	2.36	2.72	1.88	2.71	1.47	2.78	2.16	2.11	2.08	2.92	2.76	2.44	2.39	1.93
Ab	69.03	69.54	67.04	69.88	72.92	29.28	73.36	71.58	60.96	69.80	71.04	70.13	70.80	56.86	68.04	50.79	72.06	71.34	72.87	70.80	74.33	67.33	72.14	59.97	70.09	65.45	65.01	63.78	71.55	69.95	67.79	66.87	60.37
An	27.85	27.61	30.26	27.20	23.93	38.98	23.68	25.40	37.05	27.10	26.18	27.23	26.38	41.28	29.35	48.37	25.24	26.06	24.30	26.84	22.96	30.77	25.14	38.56	27.11	32.38	32.86	34.14	25.53	27.27	29.76	30.74	37.70

Al*: Al/(Ca + Na + K) a.p.f.u (excess of aluminum, Williamson et al., 2016).

Table 4
Representative electron microprobe analyses of amphibole from Altar North plutons.

Intrusion	Altar North Barren porphyry							
Sample	A156-C1							
Analysis	1	2	3	4	5	6	7	8
SiO_2	47.13	45.51	46.31	47.26	47.51	47.26	48.12	47.17
TiO_2	0.97	1.32	1.12	1.09	1.11	1.31	1.22	1.06
Al_2O_3	7.70	9.04	8.50	7.96	7.45	8.03	7.35	8.38
Cr_2O_3	0.00	0.02	0.00	0.01	0.04	0.00	0.01	0.02
FeO	13.93	14.35	14.50	13.82	13.05	13.21	13.79	13.89
MnO	0.43	0.54	0.47	0.35	0.41	0.38	0.47	0.51
MgO	14.07	13.05	13.43	14.43	14.83	14.46	14.14	13.53
CaO	11.22	11.23	11.25	10.97	11.67	11.45	11.32	11.38
Na_2O	1.80	1.95	1.92	1.92	1.64	1.79	1.58	1.72
K_2O	0.48	0.56	0.62	0.45	0.47	0.42	0.48	0.44
Cl	0.06	0.06	0.10	0.09	0.04	0.06	0.05	0.05
F	0.17	0.28	0.21	0.17	0.19	0.34	0.01	0.22
Total	97.95	97.89	98.37	98.51	98.39	98.69	98.54	98.37
No. of oxygens: 23								
Structural formulae								
Si	6.81	6.64	6.71	6.76	6.83	6.78	6.90	6.81
^{IV}Al	1.19	1.36	1.29	1.24	1.17	1.22	1.10	1.19
^{VI}Al	0.13	0.20	0.16	0.11	0.09	0.14	0.14	0.23
Ti	0.11	0.15	0.12	0.12	0.12	0.14	0.13	0.11
Cr	0.00	0.00	0.00	0.00	0.00	0.00	0.00	0.00
Fe^{3+}	0.78	0.70	0.74	0.91	0.71	0.71	0.70	0.64
Fe^{2+}	0.90	1.05	1.02	0.74	0.86	0.88	0.95	1.03
Mn	0.05	0.07	0.06	0.04	0.05	0.05	0.06	0.06
Mg	3.03	2.84	2.90	3.08	3.18	3.09	3.02	2.91
Ca	1.74	1.76	1.75	1.68	1.80	1.76	1.74	1.76
Na	0.50	0.55	0.54	0.53	0.46	0.50	0.44	0.48
K	0.09	0.10	0.11	0.08	0.09	0.08	0.09	0.08
OH^-	1.91	1.86	1.88	1.90	1.91	1.83	1.98	1.89
Cl	0.01	0.01	0.02	0.02	0.01	0.01	0.01	0.01
F	0.08	0.13	0.10	0.08	0.08	0.16	0.01	0.10
Total	17.33	17.41	17.40	17.30	17.34	17.33	17.27	17.32

minerals have slightly higher Pb isotopic ratios than the Miocene porphyritic stocks (Fig. 12b).

6. Discussion

6.1. Geochronology

U–Pb ages of rocks from the Altar area record three main episodes of igneous activity: (1) a late Carboniferous to early Permian (297.5 ± 4.2 Ma) tonalite batholith (Maydagán, 2012); (2) an early Miocene (21.6 ± 1.2 Ma, 20.8 ± 0.3 Ma; Maydagán et al., 2011, 2014; Maydagán, 2012; 21.9 ± 0.2 Ma, Gatzoubaros et al., 2014) volcanic and volcaniclastic sequence, and (3) middle to late Miocene (11.98 ± 0.1 Ma, 8.9 ± 0.4 Ma; Maydagán et al., 2014; this paper) dikes, stocks, and breccias, including intrusions related to porphyry and epithermal copper-gold mineralization.

The new U–Pb ages on zircons from AN (11.98 ± 0.19 Ma) and QDM (11.91 ± 0.33 Ma) porphyritic intrusions overlap within uncertainties with the U–Pb zircon ages of porphyry 1 (11.75 ± 0.24 Ma) and porphyry 2 (11.68 ± 0.27 Ma), both located in the eastern sector of the Altar project (Altar East). Based on these ages, the subvolcanic intrusions of AN and QDM prospects would have been emplaced in the early stages of formation of the Altar district, contemporary with the Altar East intrusions.

Some zircon crystals may have crystallized before from the same magmatic system (Chiaradia et al., 2013). Following the terminology of Miller et al. (2007), these antecrystic zircons may record the deep-seated evolution and zircon recycling in a magmatic system over several 100s of ka before final crystallization (Miller et al., 2007). LA-ICP-MS is shown to capture important first order features on the distribution of the zircon dates (Chelle-Michou et al., 2014). Zircons from Altar North and Quebrada de la Mina indicate long lived magmatism prior to porphyry emplacement, from 13.4 to 11.1 Ma (Digital Appendices A and B). The previously published ages for Altar East and Altar Central porphyry centers, together with the new ages for AN and QDM porphyritic intrusions, range between ~12 and 8.9 Ma, implying that these spatially distinct magmatic centers were emplaced within ~3 Ma.

Old ages recognized in zircon crystals from the Altar porphyries (Table 7) are consistent with xenocrysts derived from the basement of this region. The zircon xenocrysts from Altar Central and East intrusions have ages of ~297 Ma and 210 to 204 Ma respectively (Maydagán et al., 2014), which suggest that the middle to late Miocene magmas interacted with late Carboniferous to early Permian, and late Triassic crust. The tonalite batholith that is exposed to the east of the Altar project is Carboniferous to early Permian in age (297.5 ± 4.2 Ma; Maydagán, 2012).

A zircon with an age of 69.3 ± 1.85 Ma from QDM intrusion is interpreted as a xenocryst and reflects incorporation of late Cretaceous wall rocks. Volcanic rocks and intrusions of the Cretaceous magmatic episode are represented to the west of the study area, in the limit between Chile and Argentina (Fig. 2). Thus, these xenocrysts in the Altar porphyritic stocks reflect the assimilation of crustal rocks in the middle to late Miocene magmas.

6.2. Geochemistry

Trace and rare earth elements of the barren AN stock and QDM porphyry have strong similarities with Altar East and Altar Central porphyries, indicating a similar magmatic origin for the magmas. High Sr/Y ratios and listric-shaped REE patterns suggest that the magmas were equilibrated with a residual mineralogy dominated by amphibole or amphibole ± garnet (e.g. Kay et al., 1991) whereas the absence of negative Eu anomalies may be due to high magmatic oxidation states and/or suppression of plagioclase fractionation due to high pH_2O conditions (e.g. Frey et al., 1978; Kay et al., 1991; Lang and Titley, 1998; Richards et al., 2001).

Detailed studies of plagioclase profiles have been widely used to characterize magmatic processes in subduction-related systems (e.g. Singer et al., 1995; Hattori and Sato, 1996; Davidson and Tepley, 1997; Tepley et al., 2000; Davidson et al., 2001; Andrews et al., 2008). In the AN barren porphyry most plagioclase phenocrysts show outer edges with higher anorthite contents (Fig. 10). Variations in H_2O content, due to the influx of external fluids or degassing of the magma chamber, may affect An zoning of plagioclase, higher water contents typically resulting in higher An contents (e.g. Hattori and Sato, 1996; Ginibre et al., 2007). Repeated small compositional changes (An 1–10 mol%) are interpreted to reflect near-equilibrium, incremental diffusion-controlled growth occurring in a closed-system (e.g. Pearce and Kolisnik, 1990; Singer et al., 1995). Greater compositional amplitudes (An 15–20 mol%) in adjacent zones that correlate positively with significant changes in Fe and Sr, as observed in plagioclase from AN barren porphyry, reflect disturbances of the magma chamber under open-system conditions (e.g. Singer et al., 1995; Hattori and Sato, 1996; Davidson and Tepley, 1997; Tepley et al., 2000; Davidson et al., 2001; Cao et al., 2014). In addition, correlated variations of An (mol%) and FeO contents in plagioclase from the AN barren porphyry are interpreted as reflecting a process of recharge by a less evolved magma (e.g., Ginibre et al., 2007; Cao et al., 2014; Fig. 10c).

In QDM porphyry and Altar Central mineralized porphyries, the correlation between FeO contents and An (mol%) is not

Table 5
Representative electron microprobe analyses of biotite from QDM porphyry.

Sample	A1014-C3					A1014-C4			A1014-C5	
Analysis	30	31	32	33	34	43	44	45	62	63
SiO_2	37.01	36.49	37.27	37.11	36.47	37.22	37.24	36.81	36.56	36.28
TiO_2	3.67	3.51	3.54	3.48	3.71	3.18	3.34	3.10	3.41	3.61
Al_2O_3	14.82	14.48	14.80	14.91	15.06	15.02	14.60	15.01	14.35	14.72
Cr_2O_3	0.00	0.01	0.00	0.00	0.00	0.00	0.04	0.00	0.00	0.00
FeO	12.38	11.18	12.92	12.04	13.25	12.02	12.10	12.57	12.19	12.40
MnO	0.24	0.19	0.24	0.30	0.27	0.28	0.27	0.26	0.35	0.31
MgO	16.45	16.82	16.60	16.44	15.63	17.03	17.48	16.91	16.45	16.32
CaO	0.00	0.00	0.00	0.01	0.00	0.00	0.02	0.00	0.00	0.00
Na_2O	0.31	0.32	0.41	0.20	0.32	0.27	0.33	0.31	0.43	0.44
K_2O	8.86	8.99	8.75	8.89	8.62	8.80	8.81	8.73	8.72	8.68
Cl	0.15	0.17	0.12	0.18	0.11	0.10	0.11	0.09	0.10	0.13
F	1.73	2.13	1.57	1.78	1.65	1.90	1.99	2.35	1.54	1.63
H_2O	3.14	2.89	3.25	3.10	3.16	3.09	3.05	2.86	3.18	3.14
Subtotal	98.74	97.17	99.46	98.41	98.25	98.90	99.39	99.00	97.28	97.66
O = F, Cl	0.76	0.93	0.69	0.79	0.72	0.82	0.86	1.01	0.67	0.72
Total	97.98	96.24	98.77	97.63	97.53	98.08	98.53	97.99	96.61	96.95
Si	5.55	5.56	5.55	5.57	5.51	5.56	5.55	5.52	5.56	5.51
^{IV}Al	2.45	2.44	2.45	2.43	2.49	2.44	2.45	2.48	2.44	2.49
^{VI}Al	0.17	0.15	0.15	0.21	0.20	0.20	0.11	0.18	0.13	0.14
Ti	0.41	0.40	0.40	0.39	0.42	0.36	0.37	0.35	0.39	0.41
Cr	0.00	0.00	0.00	0.00	0.00	0.00	0.00	0.00	0.00	0.00
Fe	1.55	1.42	1.61	1.51	1.67	1.50	1.51	1.58	1.55	1.57
Mn	0.03	0.02	0.03	0.04	0.03	0.04	0.03	0.03	0.05	0.04
Mg	3.68	3.82	3.68	3.68	3.52	3.79	3.88	3.78	3.73	3.69
Ca	0.00	0.00	0.00	0.00	0.00	0.00	0.00	0.00	0.00	0.00
Na	0.09	0.10	0.12	0.06	0.09	0.08	0.09	0.09	0.13	0.13
K	1.69	1.75	1.66	1.70	1.66	1.68	1.67	1.67	1.69	1.68
OH^-	3.14	2.93	3.23	3.11	3.18	3.08	3.03	2.86	3.23	3.18
Cl	0.04	0.04	0.03	0.05	0.03	0.03	0.03	0.02	0.03	0.03
F	0.82	1.02	0.74	0.84	0.79	0.90	0.94	1.12	0.74	0.78
Total	19.62	19.66	19.65	19.59	19.60	19.64	19.68	19.68	19.67	19.67
Y total	5.84	5.82	5.87	5.83	5.85	5.89	5.91	5.92	5.85	5.86
X total	1.79	1.84	1.78	1.76	1.75	1.76	1.77	1.76	1.82	1.81
Al total	2.62	2.60	2.60	2.64	2.68	2.64	2.56	2.65	2.57	2.63
Fe/(Fe + Mg)	0.30	0.27	0.30	0.29	0.32	0.28	0.28	0.29	0.29	0.30
FeO + MnO	12.61	11.37	13.16	12.33	13.52	12.30	12.37	12.83	12.54	12.71

obvious (Fig. 11c). However, some small and unfractured plagioclase phenocrysts from QDM mineralized porphyry show a rim enriched in anorthite (amplitude of An 15 mol%, Fig. 11a) that suggest a magmatic recharge episode (Fig. 11). We argue that the rims enriched in anorthite, Fe and Sr recognized in both the porphyries from the study area are evidences of magma recharge processes in the magmatic chambers by a less evolved magma. These evidences are manifested more clearly in the large barren porphyries that precede mineralizing events (Fig. 10c).

Williamson et al. (2016) indicated that the excess of aluminum in plagioclase, as recognized in Altar phenocrysts, may exclude copper from these crystals, enriching in copper the remaining melts. These authors proposed that the aluminum enrichment in plagioclase may record injections of hydrous fluid or fluid-rich

Table 6
Isotopic data of Altar North, QDM, Altar Central and Altar East subvolcanic intrusions and ore minerals.

Deposit	Altar North	Quebrada de la Mina	Altar North	Altar North	Altar Central	Altar Central	Altar East
Lithologie	AN mineralized porphyry	QDM porphyry	AN barren porphyry	Breccia	Porphyry 4	pyrite (E vein)	galena (E vein)
Sample	ALD-160-232	QMD-21-243	A-13-13	GO-106	A-1-07	ALD-2-65	ALD-4-446
$^{87}Sr/^{86}Sr$	0.7046	0.7045	0.7046	0.7047	0.7052	n.a	n.a
$^{143}Nd/^{144}Nd$	0.5127	0.5126	0.5126	0.5126	0.5127	n.a	n.a
$\varepsilon_{Nd}(0)$	1.0	0.2	0.2	0.1	0.3	n.a	n.a
$\varepsilon_{Nd}(t)$	1.2	0.4	0.4	0.2	0.6	n.a	n.a
T_{DM}	770	840	840	860	830	n.a	n.a
$^{206}Pb/^{204}Pb$	18.6187	18.6175	18.6201	18.6087	18.5700	18.6195	18.6177
$^{207}Pb/^{204}Pb$	15.6294	15.6276	15.6285	15.6282	15.5980	15.6269	15.6243
$^{208}Pb/^{204}Pb$	38.5587	38.5472	38.5623	38.5505	38.4530	38.5777	38.5795
Easting[a]	23,58,593	23,55,717	23,57,939	23,57,583	23,59,194	23,59,388	23,60,389
Northing[a]	65,18,396	65,17,699	65,17,446	65,18,437	65,16,893	65,17,188	65,17,055

[a] The sample location coordinates are provided in Gauss Krueger, Inchauspe (2, Fig. 3).

Please cite this article in press as: Maydagán, L., et al., Petrogenesis of Quebrada de la Mina and Altar North porphyries (Cordillera of San Juan, Argentina): Crustal assimilation and metallogenic implications, Geoscience Frontiers (2016), http://dx.doi.org/10.1016/j.gsf.2016.11.011

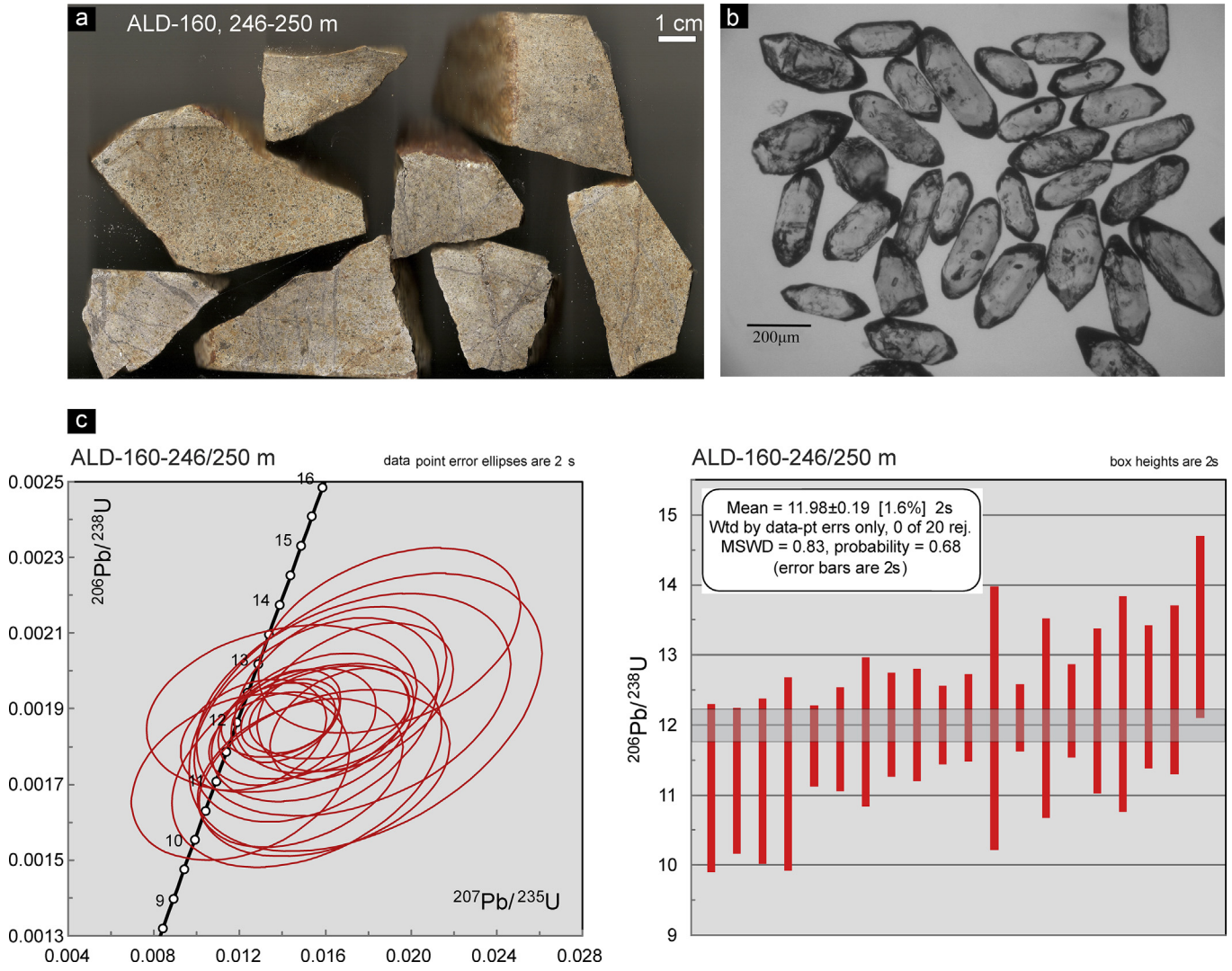

Figure 6. (a) Photographs of the rock sample from Altar North dated by LA-ICP-MS U–Pb in zircons; (b) zircons obtained from the sample; (c) U–Pb Concordia and probability diagrams of sample ALD–160–246/250 m representing AN mineralized porphyry.

melts into the sub-porphyry magma chamber (Williamson et al., 2016, Fig. 11d).

Barren AN porphyry and QDM porphyry are slightly more silicic than the porphyries of Altar East and Altar Central (Figs. 8 and 9). Compositional oscillations in Altar porphyries from felsic to more mafic and the trends of increasing and decreasing La/Sm, Sm/Yb, and Sr/Y ratios of the different intrusions over time are consistent with processes of fractionation and crystallization in the upper crustal magma chambers lying beneath and sourcing the porphyry intrusions (Hattori and Keith, 2001; Seedorff et al., 2005; Lickfold et al., 2007). The compositions of magmatic biotites from QDM porphyry indicate biotites from calc-alkaline arc tectonic environment according to the diagram of Abdel Rahman (1994).

Wu et al. (2015) studied the geochemistry, zircon trace elements and Hf isotopic compositions of the magmatic sequences of the Halasu Cu Belt, China and demonstrated a negative correlation between Ti-in-zircon temperatures and oxygen fugacity of the magmas. At Halasu Cu Belt, ore-bearing syn-mineralization intrusions are characterized by higher water content, oxygen fugacity and low temperatures with higher mineralization potential than pre- and post-mineralization intrusions (Wu et al., 2015). Most amphibole phenocrysts (edenite) from the AN barren stock are estimated to have crystallized at temperatures from 804 to 839 °C and pressures between 0.11 and 0.15 GPa from oxidized magmas ($f(O_2)$ = NNO +1.1 to +1.6) with high water contents (4.7–5.9 wt.%; Ridolfi and Renzulli, 2012, Table 8). These pressures correspond to depths of ~4 to 6 km in the upper crust (Table 8) and are similar to those previously obtained by Maydagán et al. (2014) for porphyries 1 and 5 of the Altar district.

6.3. Sr–Nd–Pb isotopes

Isotopic data of barren and mineralized AN porphyries and QDM intrusion are consistent with mixed mantle and crust contributions in their magmas. According to the Sr and Nd isotopic data, AN and QDM intrusions are slightly enriched in $\varepsilon_{Nd}(t)$ and $^{143}Nd/^{144}Nd_{(t)}$ and slightly impoverished in $^{87}Sr/^{86}Sr_{(t)}$ compared to Altar East and Altar Central intrusions (Fig. 12a). These could be explained by a greater degree of contamination of these AN and QDM magmas by the early Miocene volcanic wall-rocks, such as the basaltic andesite that has similar isotopic trends and is widespread in the study area (Fig. 12a).

Please cite this article in press as: Maydagán, L., et al., Petrogenesis of Quebrada de la Mina and Altar North porphyries (Cordillera of San Juan, Argentina): Crustal assimilation and metallogenic implications, Geoscience Frontiers (2016), http://dx.doi.org/10.1016/j.gsf.2016.11.011

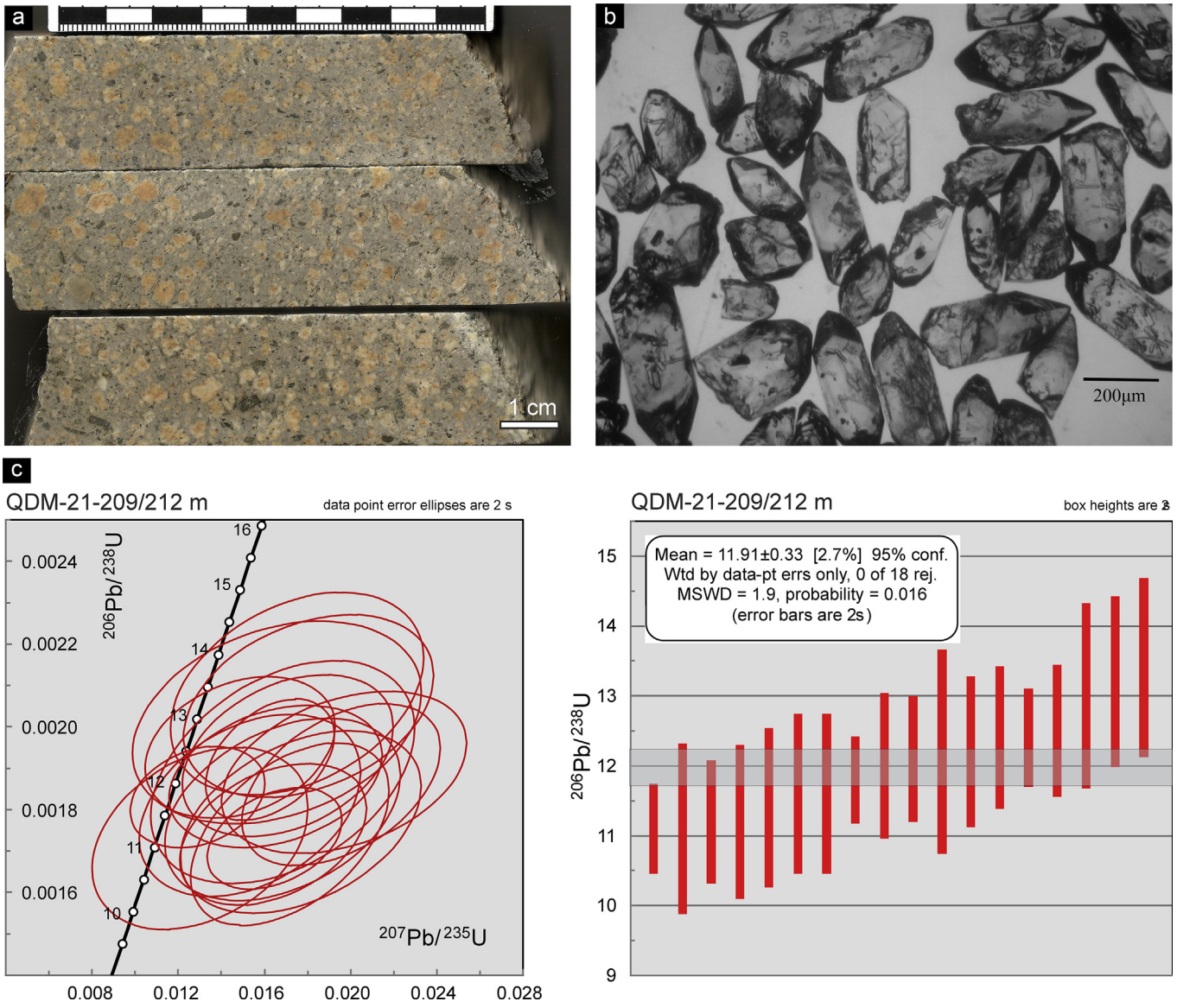

Figure 7. (a) Photographs of the rock sample from QDM porphyry dated by LA-ICP-MS U–Pb in zircons; (b) zircons obtained from the sample; (c) U–Pb Concordia and probability diagrams of sample QDM–21–209/211 m representing QDM porphyry.

Lead isotope ratios of ore minerals preserve the characteristics of their igneous host rocks in volcanic arc and rift settings (e.g. LeHuray et al., 1988), and reflect the isotopic characteristics of basement sources of Pb (e.g. Zartman, 1974; Chiaradia et al., 2004). Figs. 12b and 13 show new lead isotope data (AN and QDM intrusions and Altar mineralization), the fields of major igneous rock units of the Andes between 30° and 34°S, and lead isotopic data of ore minerals in intrusion-related deposits of this region (vein deposits, porphyry deposits and high sulfidation epithermal deposits, Tosdal and Munizaga, 2003). The AN and the QDM porphyries show very homogeneous Pb isotope ratios and are more enriched in radiogenic lead compared to the rest of the Altar intrusions. Samples from the AN and the QDM intrusions plot near the boundary between Miocene volcanic rocks and the Carboniferous to Triassic igneous rocks fields (Fig. 13a, b). Altar East intrusions have similar Pb isotope ratios to the sulfides from other porphyry Cu deposits of the Central Andes (30°–34°S; Tosdal and Munizaga, 2003), whereas AN and QDM intrusions plot in the field of high sulfidation epithermal deposits of the Central Andes (30°–34°S; Tosdal and Munizaga, 2003) characterized by a higher content of radiogenic Pb (Fig. 13c). The lead isotope ratios of the sulfides from late Altar East veins (pyrite and galena from E veins, Maydagán et al., 2015) plot within the epithermal high-sulfidation deposit field (Fig. 13c). The porphyries show a positive correlation between $^{207}Pb/^{204}Pb$ versus SiO_2 interpreted as indicative of assimilation processes coupled with magmatic differentiation, whereas the andesitic volcanic host rocks show a negative correlation between $^{207}Pb/^{204}Pb$ and SiO_2 (Fig. 13d). To explain these differences, Maydagán et al. (2014) suggested the presence of two different sources of radiogenic Pb for Altar magmas: (1) mantle-enriched with Pb-rich aqueous fluids from the subducted slab, and (2) crustal components from the basement of this region (Fig. 13d).

Fig. 14a, b shows $\varepsilon_{Nd}(t)$ versus $^{87}Sr/^{86}Sr$ and $^{87}Sr/^{86}Sr$ versus SiO_2 diagrams of the porphyries of the flat slab segment: El Teniente (34°S), Río Blanco (33°S), Los Pelambres (31.4°S), Altar

Please cite this article in press as: Maydagán, L., et al., Petrogenesis of Quebrada de la Mina and Altar North porphyries (Cordillera of San Juan, Argentina): Crustal assimilation and metallogenic implications, Geoscience Frontiers (2016), http://dx.doi.org/10.1016/j.gsf.2016.11.011

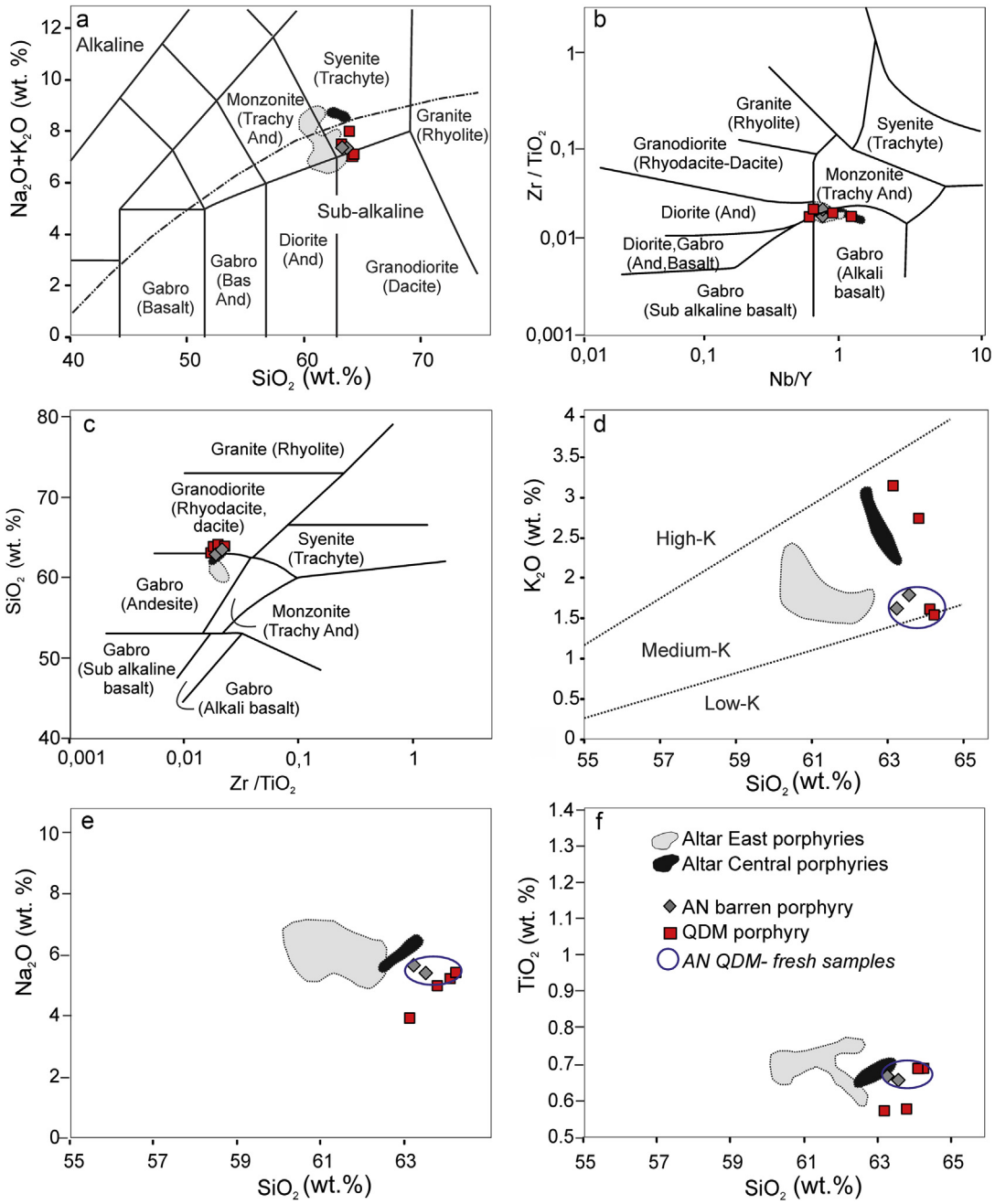

Figure 8. (a) $Na_2O + K_2O$ versus SiO_2, showing the alkaline and subalkaline fields; (b) Zr/TiO_2 versus Nb/Y diagram (modified from Winchester and Floyd, 1977); (c) SiO_2 versus Zr/TiO_2 (modified from Winchester and Floyd, 1977; equivalence between plutonic and volcanic (subvolcanic) rock names from Wu et al. (2015); (d) K_2O versus SiO_2 diagram; (e) Na_2O versus SiO_2; (f) TiO_2 versus SiO_2 for AN barren porphyry and QDM porphyry. Data of Altar East and Altar Central porphyries are from Maydagán et al. (2011) and Maydagán et al. (2014).

(31°30′S), Maricunga (26°–28°S), Farallón Negro Volcanic Complex (Bajo La Alumbrera; 27°S). The location of the porphyry deposits of the flat slab segment and its gold grades is shown in Fig. 14c. Fig. 14d shows new lead isotope data of AN and QDM porphyries with the isotope data of the igneous rocks of the flat slab segment (Kay et al., 1991; Bissig et al., 2003) and the basement lithologies of the El Indio region (Tosdal et al., 1999). AN and QDM porphyries and the mineralization plot close to the basement rocks from the El Indio region and to the El Indio-Tambo epithermal ores (Fig. 14d). Lead isotopic compositions of ore minerals from Miocene high-sulfidation epithermal deposits from El Indio and Tambo are interpreted to reflect mixing of two sources, an enriched mantle source and a radiogenic crustal source (Macfarlane, 1999). These deposits have a contribution of lead from a high $^{207}Pb/^{204}Pb$ source similar to Carboniferous to Triassic rocks, which directly underlie the deposits (Tosdal and Munizaga, 2003).

High radiogenic Pb ratios in the Altar region have been observed in the basaltic andesites of the early Miocene lower volcanic complex that have low radiogenic Sr and Nd (Maydagán et al., 2011) and in the tonalite of Carboniferous age corresponding to the basement rocks of this region (Maydagán, 2012; Fig. 13d). Zircon xenocrysts with similar ages to the tonalite (~297 Ma) found in Altar porphyritic intrusions together with xenocrysts of Triassic

Please cite this article in press as: Maydagán, L., et al., Petrogenesis of Quebrada de la Mina and Altar North porphyries (Cordillera of San Juan, Argentina): Crustal assimilation and metallogenic implications, Geoscience Frontiers (2016), http://dx.doi.org/10.1016/j.gsf.2016.11.011

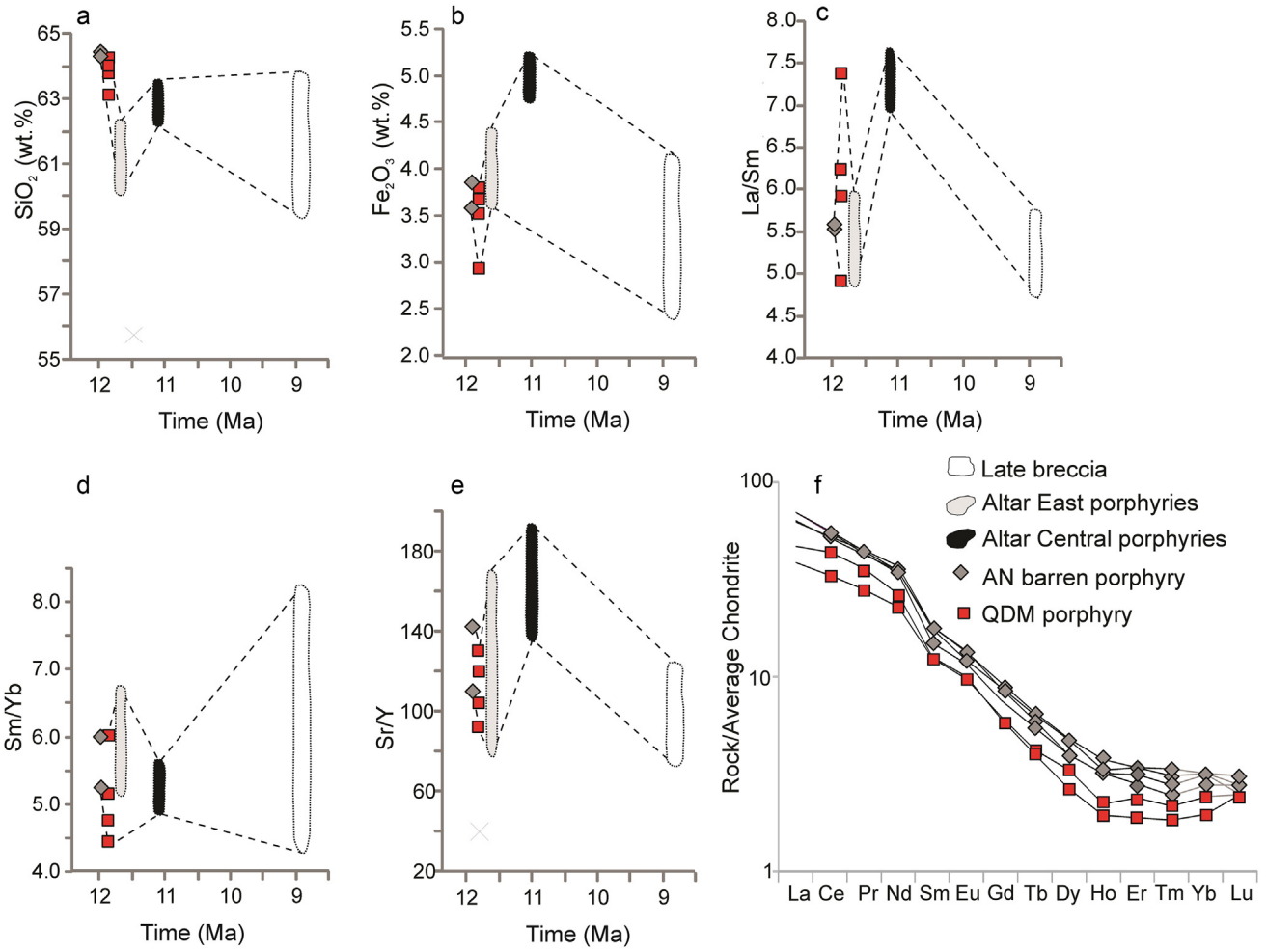

Figure 9. (a–e) Diagrams of SiO_2, Fe_2O_3, La/Sm, Sm/Yb, and Sr/Y versus time. (f) Whole-rock REE concentrations normalized to average chondrite (Boynton, 1989).

and Cretaceous ages may be related with assimilation of old igneous rocks in the Miocene magmas. Similar to the El Indio, the ore minerals analyzed from Altar Central and Altar East show a decoupling with the ores being more radiogenic than associated subvolcanic rocks (Fig. 13c). This suggests that magmatic-hydrothermal fluids that formed the mineralization in these deposits have remobilized Pb from the host basement rocks. In contrast, ore Pb isotope signatures overlap with the more radiogenic Pb isotope compositions of the magmas from AN and QDM, suggesting that in this case magmas have assimilated basement rocks before exsolving the hydrothermal fluids.

6.4. Metallogenic implications

Most porphyry Cu deposits are spatially and genetically related to highly oxidized, magnetite-series I-type granitoids (Hedenquist and Lowenstern, 1994; Audétat et al., 2004; Sillitoe, 2010). Porphyries contain large quantities of sulfur as copper sulfide minerals and they can be considered as huge sulfur anomalies (Hunt, 1977). Felsic melts have a low solubility for sulfur (Wallace and Carmichael, 1992) whereas mafic melts have a great capacity to transfer sulfur from the mantle to the shallow crust as a result of their high sulfur solubility (Hattori and Keith, 2001).

Sulfide saturation can produce metal-enriched regions in the magmatic chambers (Wilkinson, 2013). When hotter mafic melt intrudes into the chamber it produces escapes of the magma forming cylindrical intrusions accompanied by exsolution and upward release of volatile and gases (e.g. Keith et al., 1997; Chiaradia et al., 2012). If such events coincide with a region of previous sulfide saturation, the conditions could be optimized for porphyry ore formation (Wilkinson, 2013). If not, this mechanism produces barren or low-grade intrusions that commonly occur in fertile systems (Wilkinson, 2013).

Blundy et al. (2015) proposed that copper enrichment initially involves metalliferous, magmatic hyper-saline liquids, or brines, that exsolve from large, magmatic intrusions assembled in the shallow crust over tens to hundreds of thousands of years. In a subsequent step, sulfide ore precipitation is triggered by the interaction of the accumulated brines with sulfur rich gases, liberated in short-lived bursts from the underlying mafic magmas. In the light of the above studies and the evidences shown here for mafic magma recharges occurring in the mineralization-related magmatic system of Altar, we argue that mafic recharges observed in the Altar system could have played a direct role in the mineralizing process (adding fluids, sulfur, copper) or an indirect role (thermal rejuvenation, sulfide mobilization) favoring the formation of this large ore deposit.

6.5. Crustal assimilation and gold content in the magmas

Differences in the isotopic ratios observed in the porphyries of the flat slab segment (Fig. 14a, b) reflect an increase in the amount

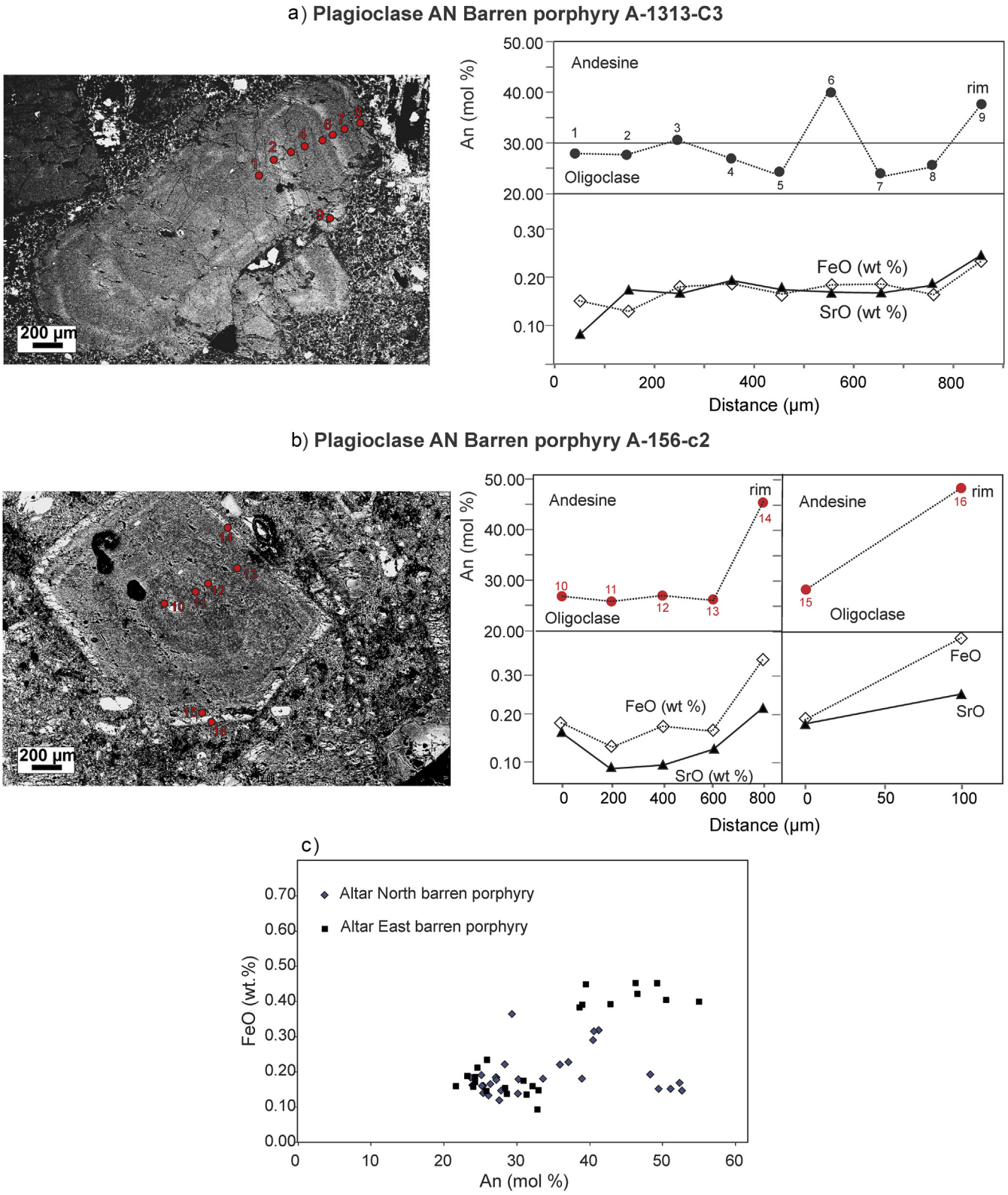

Figure 10. (a–b) BSE images of a plagioclase phenocrysts of the barren AN barren porphyry with compositional zonation and profiles of compositional variation of anorthite (mol%), FeO* (wt.%) and SrO, which provide evidence of magmatic recharge. (c) FeO (wt.%) versus An (mol%) in plagioclase of AN barren porphyry and Altar East barren porphyry. Data of Altar East porphyry is from Maydagán et al. (2014).

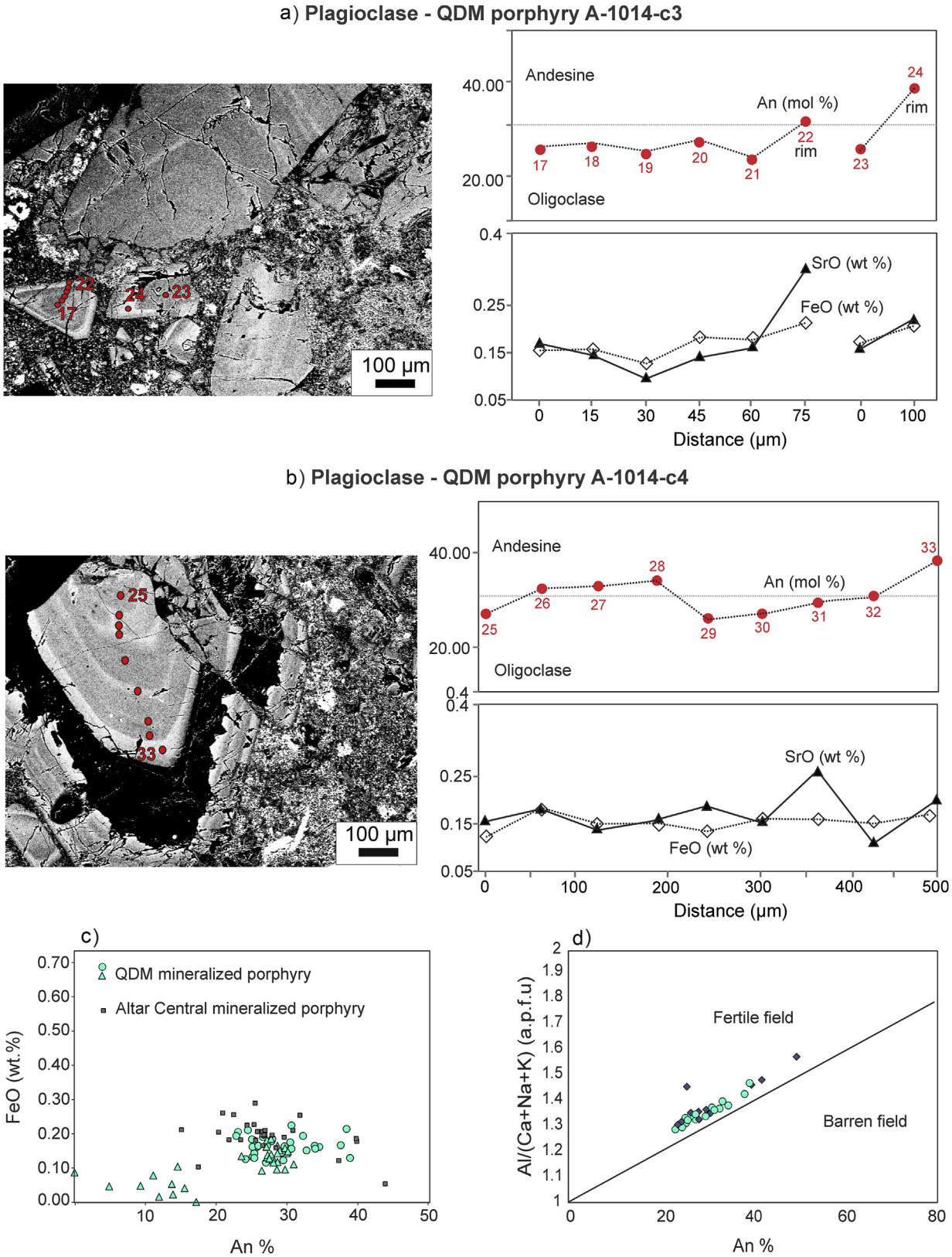

Figure 11. (a–b) BSE images of plagioclase phenocrysts of the QDM porphyry with compositional zonation and profiles of compositional variation of anorthite (mol%), FeO* (wt.%) and SrO (wt.%). (c) FeO (wt.%) versus An (mol%) in plagioclase of QDM mineralized porphyry and Altar Central mineralized porphyry. Data of Altar Central porphyry is from Maydagán et al. (2014). (d) Al/(Ca + Na + K) versus anorthite (%) in plagioclase from QDM and AN porphyries.

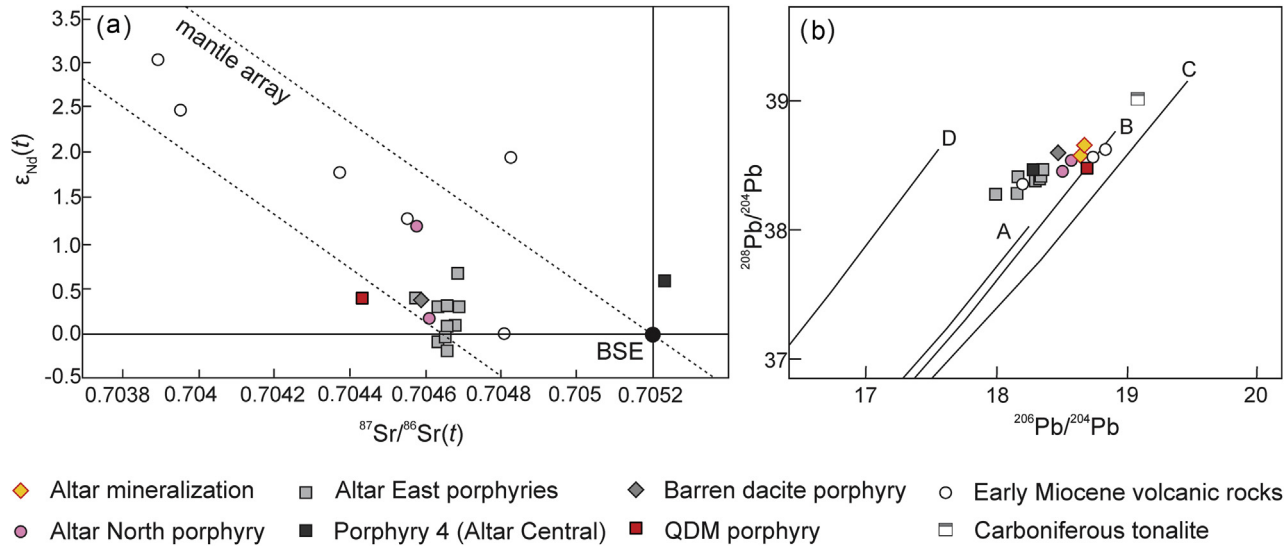

Figure 12. (a) $\varepsilon_{Nd}(t)$ versus $^{87}Sr/^{86}Sr_{(t)}$ isotope correlation diagram for AN and QDM samples showing the mantle array and the BSE (bulk silicate earth). (b) $^{208}Pb/^{204}Pb$ versus $^{206}Pb/^{204}Pb$ isotope correlation diagram of Zindler and Hart (1986) generated by the plumbotectonics model for the mantle (A), orogene (B), upper crust contributed to the orogene (C), and lower crust contributed to the orogene (D). Data of Altar East and Altar Central porphyries are from Maydagán et al. (2011) and Maydagán et al. (2014).

Table 7
Ages of zircon xenocryts from Altar samples.

Deposit	Intrusion	Xenocryst age (Ma)	Error (Ma)	Age
Altar East	Porphyry 1	210.7	4.4	Late Triassic
	Porphyry 1	204.6	2.7	Late Triassic
	Porphyry 2	297.5	3	Late Carboniferous
Altar Central	Porphyry 4	226.7	1.7	Late Triassic
	Porphyry 4	201.5	1.8	Late Triassic
QDM	QDM porphyry	69.3	1.85	Late Cretaceous

Table 8
Physical and chemical conditions for Altar North magmas based on the amphibole compositions.

Intrusion	Altar North barren porphyry							
Sample	A156-C1							
Analysis	1	2	3	4	5	6	7	8
T (°C)	818	854	839	822	823	831	804	826
Uncertainty (σest)	22	22	22	22	22	22	22	22
P (MPa)	127	180	155	132	118	135	115	149
kbars	1.3	1.8	1.5	1.3	1.2	1.4	1.1	1.5
Uncertainty (Max error)	14	20	17	15	13	15	13	16
Continental depth (km)	5	7	6	5	4	5	4	6
ΔNNO	1.4	1.0	1.1	1.5	1.6	1.4	1.4	1.2
log $f O_2$	−12.0	−11.8	−11.9	−11.9	−11.8	−11.8	−12.4	−12.1
Uncertainty (σest)	0.4	0.4	0.4	0.4	0.4	0.4	0.4	0.4
H_2O melt (wt.%)	5.0	5.7	5.1	4.9	4.7	5.2	5.1	5.9
Uncertainty	0.4	0.4	0.4	0.4	0.4	0.4	0.4	0.4

Notes: The parameters were calculated according to the work of Ridolfi and Renzulli (2012).

of radiogenic components incorporated into magmas from south to north, which correlate with an increase of crustal thickness (El Teniente ~30–35 km, El Indio >55 km, Kay et al., 1991). An improved depth to actual Moho map confirms this variation: 65–74 km of thickness north of 31°S, 55–65 km between 31° and 33°S, and 45–49 km between 33° and 34°S (Gans et al., 2011). The origin of the radiogenic components could be explained by intracrustal contamination processes (MASH; Hildreth and Moorbath, 1988) related with the interaction of the magmas with a thicker crust, source region contamination by subduction erosion (e.g., Stern, 1991) or by a combination of intracrustal and source region contamination processes (Kay et al., 2005). Recently in-situ analysis of O and Hf isotopes in zircon demonstrates that the assimilation of pre-existing continental crust plays a dominant role (over contamination of mantle wedge by subducting components or subduction erosion) in modifying the isotopic composition of late Eocene to late Miocene mantle-derived magmas (Jones et al., 2015).

Flat Slab porphyries show increased assimilation of radiogenic components in the magmas from south to north evidenced by Sr and Nd isotopes (Fig. 14a). The positive correlation of $^{87}Sr/^{86}Sr$ versus SiO_2 indicates the assimilation processes were associated with magmatic differentiation in the magmas (Fig. 14b). Increasing $^{207}Pb/^{204}Pb$ values that are not accompanied by time integrated growth of $^{206}Pb/^{204}Pb$ are interpreted to imply assimilation of crustal rocks in the melts as they traversed the thickened crust (Hildreth and Moorbath, 1988; Kay and Abbruzzi, 1996). At Agua Rica deposit sulfides, and hydrothermal breccias show Pb isotope signatures more radiogenic than Cenozoic igneous rocks of this area. They are therefore indicative of interaction between the magmatic fluid and the Eopaleozoic basement rocks of the Agua Rica deposit (Liska Borba et al., 2016) as suggested by the Pb isotope ratios of the Eopaleozoic Capillitas Granite (Tilton et al., 1981).

Gold grades in the Flat Slab deposits increase from south to north (El Teniente 0.005 g/t, Los Pelambres 0.03 g/t; Altar 0.06 g/t; Agua Rica 0.23 g/t; Maricunga 0.4 g/t; Bajo La Alumbrera 0.64 g/t (Singer et al., 2008; Maydagan et al., 2014 and references therein; Fig. 14c). $^{207}Pb/^{204}Pb$ ratios increase from the porphyries located south of Altar (El Teniente, Río Blanco) to the deposits located in the northern sector (El Indio-Tambo, Maricunga, Bajo la Alumbrera), that coincide with an increase of Au content of these magmas (Fig. 14c, d). Titley (1991) noted an apparent basement control on

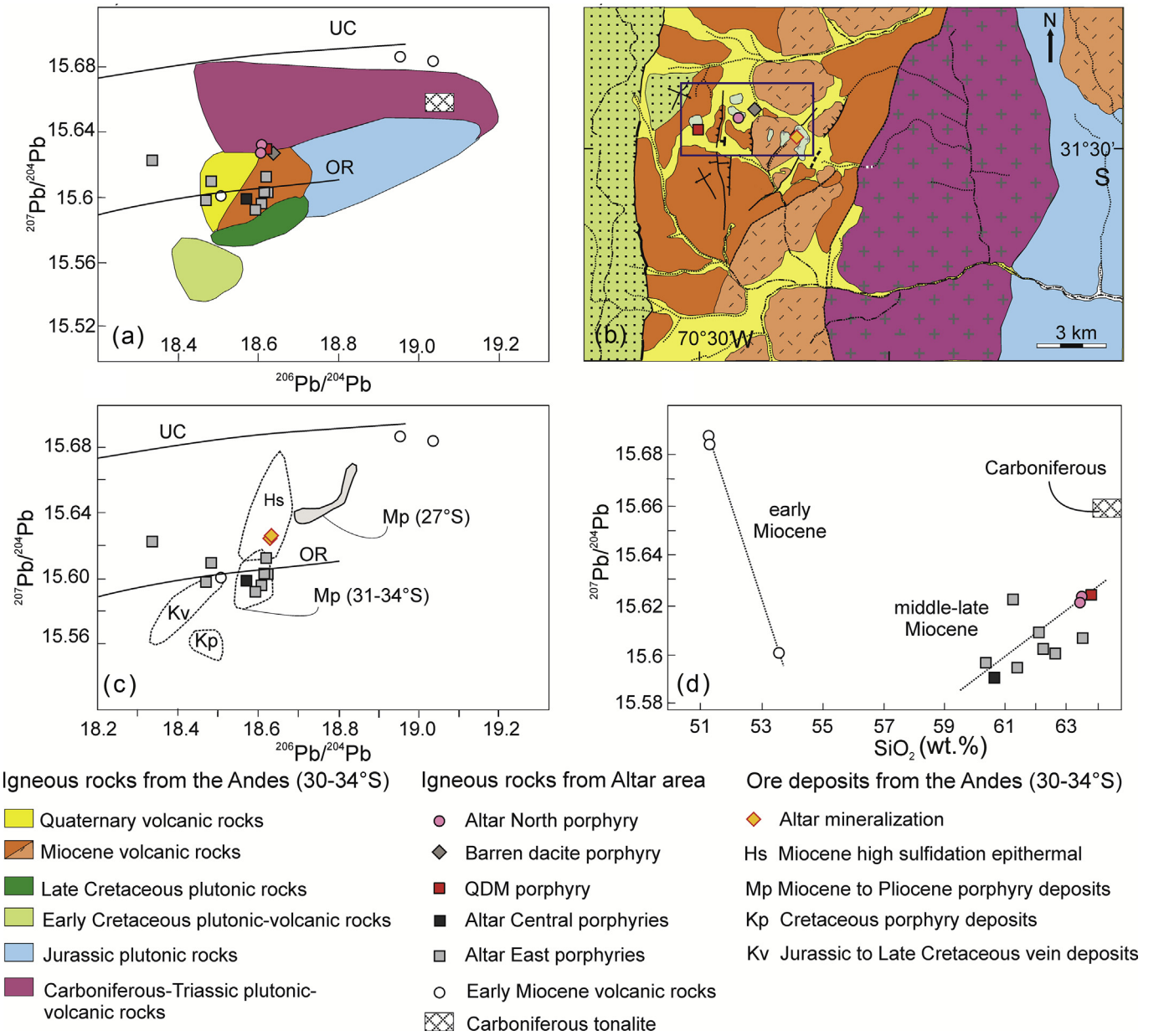

Figure 13. (a) $^{207}Pb/^{204}Pb$ versus $^{206}Pb/^{204}Pb$ diagrams showing the fields for the major igneous rock units. Quaternary rocks are from Hildreth and Moorbath (1988), the Miocene field is from Tilton (1979), Kay and Abbruzzi (1996), Kurtz et al. (1997), and Kay et al. (1999). Carboniferous to Triassic, Jurassic, Cretaceous, and latest Cretaceous data is from Gana and Tosdal (1996), and Martin et al. (1995, 1999). Early Miocene Altar volcanic rocks, Altar East and Altar Central porphyries is from Maydagán et al. (2014). (b) Geologic map of Altar area and location of Pb isotope samples. (c) $^{207}Pb/^{204}Pb$ versus $^{206}Pb/^{204}Pb$ diagrams of ore minerals in Andean intrusion-related deposits. Miocene high sulfidation epithermal, Miocene to Pliocene porphyry deposits (31°–34°S), Cretaceous porphyry deposits and Jurassic to late Cretaceous veins are from Tosdal and Munizaga (2003) and references therein. Miocene to Pliocene porphyries (27°S, Agua Rica and Bajo La Alumbrera) are from Liska Borba et al. (2016). (d) $^{207}Pb/^{204}Pb$ versus SiO_2 diagram for Altar samples (explanations in the text).

Please cite this article in press as: Maydagán, L., et al., Petrogenesis of Quebrada de la Mina and Altar North porphyries (Cordillera of San Juan, Argentina): Crustal assimilation and metallogenic implications, Geoscience Frontiers (2016), http://dx.doi.org/10.1016/j.gsf.2016.11.011

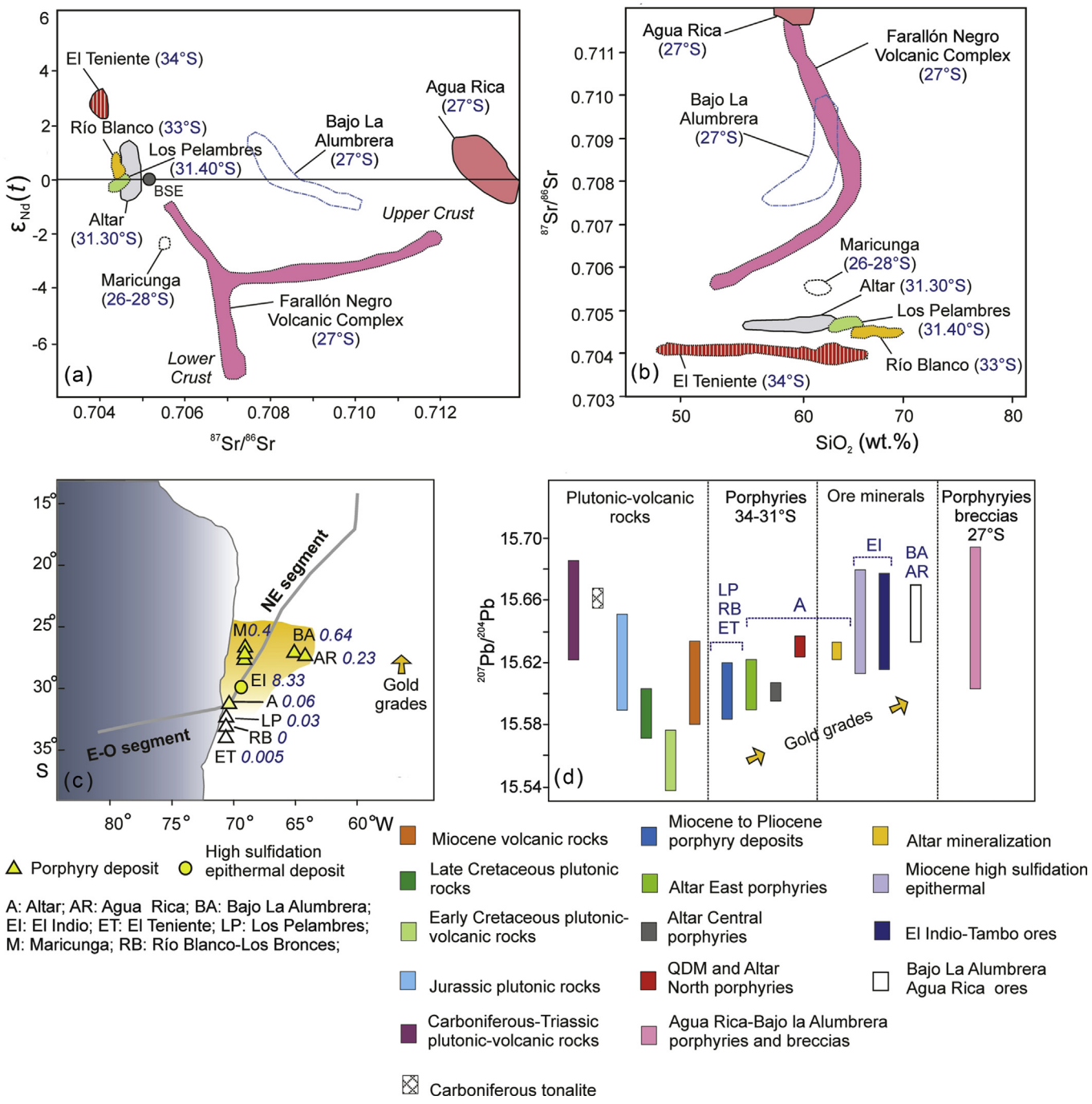

Figure 14. (a-b) $\varepsilon_{Nd}(t)$ versus $^{87}Sr/^{86}Sr$ and $^{87}Sr/^{86}Sr$ versus SiO_2 of the porphyries of the flat slab segment: El Teniente (34°S; Stern et al., 2010), Río Blanco (33°S; Serrano et al., 1996), Los Pelambres (31.4°S; Reich et al., 2003), Altar (31.3°S; Maydagán et al., 2014; this study), Maricunga (26°–28°S; Kay et al., 1999), Farallon Negro Volcanic Complex (27°S; Halter et al., 2004), Agua Rica and Bajo La Alumbrera (27°S, Liska Borba et al., 2016). (c) The location of the porphyry deposits of the flat slab segment and its gold grades (Singer et al., 2008; Marek, 2014; Maydagán et al., 2014 and references therein; www.alumbrera.com.ar; www.yamana.com). (d) New lead isotope data of AN and QDM porphyries and ore minerals with the isotope data of igneous rocks and ore deposits of the region (Kay et al., 1991, 1999; Serrano et al., 1996; Tosdal et al., 1999; Bissig et al., 2003; Reich et al., 2003; Tosdal and Munizaga, 2003; Halter et al., 2004; Stern et al., 2010; Maydagán et al., 2014; Liska Borba et al., 2016).

Please cite this article in press as: Maydagán, L., et al., Petrogenesis of Quebrada de la Mina and Altar North porphyries (Cordillera of San Juan, Argentina): Crustal assimilation and metallogenic implications, Geoscience Frontiers (2016), http://dx.doi.org/10.1016/j.gsf.2016.11.011

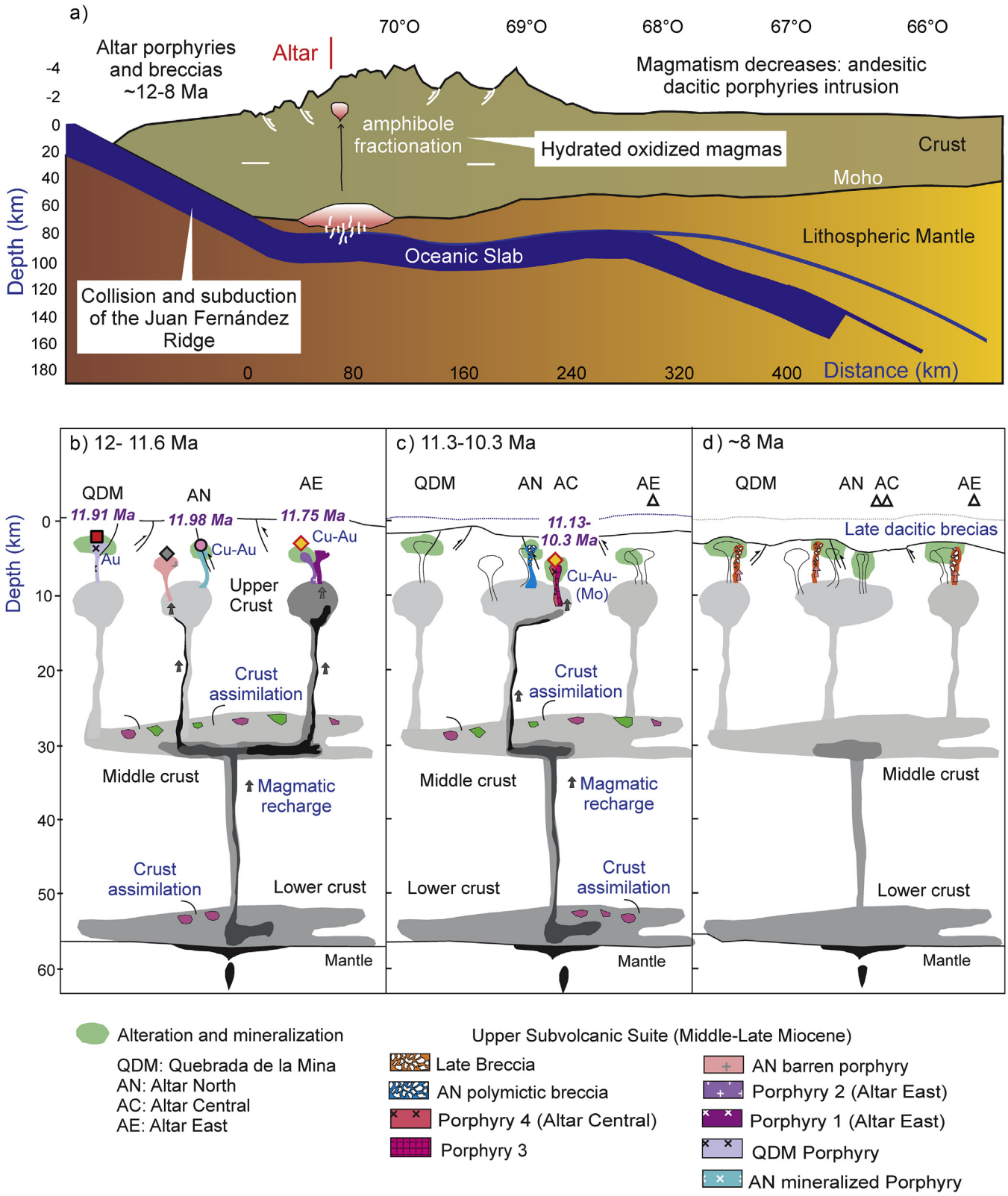

Figure 15. (a) Schematic lithospheric-scale cross section of the study area during the middle-late Miocene. (b–d) Model of the evolution of the magmatic-hydrothermal centers of the Altar mining district (explanations in the text).

Please cite this article in press as: Maydagán, L., et al., Petrogenesis of Quebrada de la Mina and Altar North porphyries (Cordillera of San Juan, Argentina): Crustal assimilation and metallogenic implications, Geoscience Frontiers (2016), http://dx.doi.org/10.1016/j.gsf.2016.11.011

precious metal contents in Arizona mineral deposits. Tosdal (1995) suggested that there might be a crustal influence on the precious metal content, principally Au content, in ore deposits. We suggest that the increase in the content of Au in the magmas from south to north in the flat slab segment could be linked to greater assimilation of high radiogenic Pb components associated with Miocene long lived maturation systems.

The Au/Cu ratio in porphyry deposits is probably determined by a magmatic source control on metal endowment, including interaction of mafic mantle and felsic crustal melts (Halter et al., 2005). Higher Au/Cu ratio in Altar compared to the nearby Miocene porphyry deposits of Los Pelambres, Pachón, Río Blanco and Los Bronces suggest that gold concentration may be associated with increased interaction and contamination in Altar magmas with high radiogenic Pb components derived in part from the thickened crust.

7. Petrogenetic model

Mineral deposits located in the El Indio, Altar and El Teniente regions have been emplaced under similar geodynamic conditions related to the shallowing of the slab that led to drastically reduced magmatic activity in the Cordillera Principal, compression, extinction or eastward migration of the arc (Fig. 15a). Porphyries were emplaced in a thickening crust of intermediate to mafic composition (Alvarado et al., 2007) after their parental magmas were equilibrated with hornblende or hornblende ± garnet at variably deep crustal levels (Fig. 15a).

During the Miocene, fluid released from the subducted materials provided water, sulfur, chlorine, alkalis, and other components that flux to the overlying mantle wedge and leaded to melting and generation of deep oxidized mafic precursors to the magmas (e.g. Richards, 2003; Kelley and Cottrell, 2009; Wu et al., 2015). The increased compression in the lithosphere may have hindered the upward ascent of the magmas and favored their pooling in chambers within the Miocene thickened crust (e.g., Richards et al., 2001; Richards, 2003; Chiaradia et al., 2009). We argue that long-lived and large magmatic chambers in Altar were located in the lower and middle crust (Fig. 15b). In these chambers, the magmas evolve to form hydrous, oxidized, and sulfur-rich arc andesites and dacites characterized by high Sr/Y via fractionation of amphibole ± garnet (e.g. Kay and Mpodozis, 2002; Chiaradia et al., 2009; Loucks, 2014). Sustained crustal magmatism appears to have favored crustal assimilation (basement and previous volcanic rocks). The long-lived magmatic system in Altar experienced magmatic recharge episodes by hotter and more mafic magmas from the lower crust. The latter might have also provided additional metal and volatile contributions.

We argue that the collision of the Juan Fernandez Ridge with the trench at ~11 Ma and the subduction of the Juan Fernández Ridge beneath Altar region at ~11–10 Ma (Yañez et al., 2001; Maydagán et al., 2011) may have promoted changes in the tectonic stress regime, allowing the magmas to rise to shallower levels in the crust. Intrusive activity began with emplacement of andesite to dacite intrusions at AN, QDM and Altar East porphyry centers (11.98 ± 0.1, 11.91 ± 0.3 and 11.75 ± 0.24 Ma, Fig. 15b). In a subsequent stage, the Altar Central porphyry center was formed (11.13 ± 0.26 and 10.35 ± 0.32 Ma, Fig. 15c). After the emplacement of porphyry 4 and during the hydrothermal lifetime of the central orebody, exhumation and erosion would have favored the overlapping of the shallow and deep mineralization (Maydagán et al., 2015). In the final stage the Late Breccia was emplaced at ~8.9 Ma (Maydagán et al., 2014, Fig. 15d).

Recent geochronological studies in Los Pelambres deposit presented U–Pb ages in zircon of 12.30 ± 0.30 and 10.53 ± 0.14 Ma for the intrusions and Re-Os ages in molybdenite of 11.81 ± 0.06 and 10.14 ± 0.04 Ma (Perelló et al., 2012) stating that Los Pelambres and Altar porphyry deposits formed almost simultaneously. This supports the hypothesis that the emplacement of the mineralized intrusions is linked to a regional tectonic event such as the collision of the Juan Fernández Ridge at these latitudes.

8. Concluding remarks

The geochemical and isotopic data obtained for the porphyries of Altar North and Quebrada de la Mina show that these intrusions are genetically linked to the Altar deposit and form part of a very large magmatic-hydrothermal system. Altar North (11.98 ± 0.19 Ma) and Quebrada de la Mina (11.91 ± 0.33 Ma) porphyries have been emplaced in the early stages of formation of the Altar district.

Amphibole phenocrysts from Altar North barren porphyry crystallized from oxidized magmas (fO_2 = NNO +1.1 to +1.6) with high water contents (4.7–5.9 wt.%). Chemical analyses enriched in anorthite, Fe and Sr in zoned plagioclase of the porphyries from Altar North and Quebrada de la Mina deposits reflect episodes of recharge by a less evolved magma in the magmatic chambers.

Magmas have experienced assimilation of Miocene, Cretaceous, Triassic and Carboniferous rocks as indicated by the age of zircon xenocrysts. $^{207}Pb/^{204}Pb$ isotope data of Altar ore minerals, and of Quebrada de la Mina and Altar North intrusions match the signatures of the high-sulfidation deposits of Chile and reflect an increment of the assimilation of radiogenic Pb components in the magmas.

We suggest that the increase in Au content, from south to north, in the porphyry deposits of the flat slab segment could be linked to an increase in the assimilation of high radiogenic Pb components in the magmas within these long-lived maturation systems.

The magmatic processes that should have favored the formation of the mineralization in the Altar district are: (1) the evolution of a long-lived magmatic system in deep magma chambers during periods of compression in the crust, (2) the generation of oxidized and hydrated magmas that may have promoted the transport of large volumes of copper from deep crust levels to the upper crust magmatic chambers, (3) changes in the tectonic stress regime that allow magmas to rise to shallower levels, (4) mafic recharge events in the upper crust magmatic chambers that could play a direct role in the mineralizing process (adding fluids, sulfur, chalcophile metals) or an indirect role (thermal rejuvenation, and sulfide mobilization).

Acknowledgements

This research forms part of a project financed by CONICET (PIP 330), by Universidad Nacional del Comahue (PIN 4-I-209), and Minera Peregrine Argentina S.A.-Stillwater Mining Company. We appreciate the detailed and constructive reviews and suggestions of Wenjiao Xiao and two anonymous reviewers, which greatly improved this contribution. We express our appreciation to Ralph Green for their support to this study, to María Isabel Romero and all the staff of Peregrine Metals Ltd. for provision of site access, logistic support and help during the field work. We thank Lucas Riffo for their help during the field mapping and sampling.

Appendix A. Supplementary data

Supplementary data related to this article can be found at http://dx.doi.org/10.1016/j.gsf.2016.11.011.

References

Abdel Rahman, A.F., 1994. Nature of biotites from alkaline, calcalkaline, and peraluminous magmas. Journal of Petrology 25, 525–541.
Alvarado, P., Beck, S., Zandt, G., 2007. Crustal structure of the south-central Andes Cordillera and backarc region from regional waveform modeling. Geophysical Journal International 170, 858–875.
Anderson, M., Alvarado, P., Zandt, G., Beck, S., 2007. Geometry and brittle deformation of the subducting Nazca Plate, Central Chile and Argentina. Geophysical Journal International 171, 419–434.
Andrews, B.J., Gardner, J.E., Housh, T.B., 2008. Repeated recharge, assimilation, and hybridization in magmas erupted from El Chichón as recorded by plagioclase and amphibole phenocrysts. Journal of Volcanology and Geothermal Research 175, 415–426.
Audétat, A., Pettke, T., 2006. Evolution of a porphyry-Cu mineralized magma system at Santa Rita, New Mexico (USA). Journal of Petrology 47, 2021–2046.
Audétat, A., Pettke, T., Dolejš, D., 2004. Magmatic anhydrite and calcite in the ore-forming quartz-monzodiorite magma at Santa Rita, New Mexico (USA): genetic constraints on porphyry-Cu mineralization. Lithos 72, 147–161.
Bissig, T., Clark, A., Lee, J., Von Quadt, A., 2003. Petrogenetic and metallogenic responses to Miocene slab flattening: constraints from the El Indio-Pascua Au-Ag-Cu belt, Chile/Argentina. Mineralium Deposita 38, 844–862.
Blundy, J., Mavrogenes, J., Tattitch, B., Sparks, S., Gilmer, A., 2015. Generation of porphyry copper deposits by gas-brine reaction in volcanic arcs. Nature Geoscience. http://dx.doi.org/10.1038/NGEO2351.
Boynton, N.V., 1989. Cosmochemistry of the rare earth elements: condensation and evaporation processes. In: Lipin, B.R., MacKay, G.A. (Eds.), Geochemistry and Mineralogy of Rare Earths, Rev Mineral 21. Mineral Society of America, pp. 1–24.
Branney, M.J., Kokelaar, P., 2002. Pyroclastic Density Currents and the Sedimentation of Ignimbrites. In: Geological Society Memoir 27. Geological Society of London, London.
Cahill, T., Isacks, B., 1992. Seismicity and shape of the subducted Nazca plate. Journal of Geophysical Research 97, 17503–17529.
Cao, M., Qin, K., Li, G., Yang, Y., Evans, N.J., Zhang, R., Jin, L., 2014. Magmatic process recorded in plagioclase at the Baogutu reduced porphyry Cu deposit, western Junggar, NW-China. Journal of Asian Earth Sciences 82, 136–150.
Charrier, R., Baeza, O., Elgueta, S., Flynn, J.J., Gans, P., Kay, S.M., Muñoz, N., Wyss, A.R., Zurita, E., 2002. Evidence for Cenozoic extensional basin development and tectonic inversion south of the flat-slab segment, southern Central Andes, Chile (33°–36°S). Journal of South American Earth Sciences 15, 117–139.
Chelle-Michou, C., Chiaradia, M., Ovtcharova, M., Ulianov, A., Wotzlaw, J.F., 2014. Zircon petrochronology reveals the temporal link between porphyry systems and the magmatic evolution of their hidden plutonic roots (the Eocene Coroccohuayco deposit, Peru). Lithos 198, 129–140.
Chiaradia, M., Fontboté, L., Paladines, A., 2004. Metal sources in mineral deposits and crustal rocks of Ecuador (1N–4S): a lead isotope synthesis. Economic Geology 99 (6), 1085–1106.
Chiaradia, M., Merino, D., Spikings, R., 2009. Rapid transition to long-lived deep crustal magmatic maturation and the formation of giant porphyry-related mineralization (Yanacocha, Peru). Earth and Planetary Science Letters 288, 505–515.
Chiaradia, M., Ulianov, A., Kouzmanov, K., Beate, B., 2012. Why large porphyry Cu deposits like high Sr/Y magmas? Science Reports 2, 685. http://dx.doi.org/10.1038/srep00685.
Chiaradia, M., Schaltegger, U., Spikings, R., Wotzlaw, J.F., Ovtcharova, M., 2013. How accurately can we date the duration of magmatic-hydrothermal events in porphyry systems? An invited paper. Economic Geology 108 (4), 565–584.
Cooke, D.R., Hollings, P., Walshe, J.L., 2005. Giant porphyry deposits: characteristics, distribution, and tectonic controls. Economic Geology 100, 801–818.
Davidson, J.P., Tepley, F.J., 1997. Recharge in volcanic systems: evidence from isotope profiles of phenocrysts. Science 275 (5301), 826–829.
Davidson, J., Tepley, F.J., Palacz, Z., Meffan-Main, S., 2001. Magma recharge, contamination and residence times revealed by in situ laser ablation isotopic analysis of feldspar in volcanic rocks. Earth and Planetary Science Letters 184, 427–442.
Farías, M., Charrier, R., Carretier, S., Martinod, J., Fock, A., Campbell, D., Cáceres, J., Comte, D., 2008. Late Miocene high and rapid surface uplift and its erosional response in the Andes of central Chile (33°–35°S). Tectonics 27, TC1005. http://dx.doi.org/10.1029/2006TC002046.
Frey, F.A., Chappell, B.W., Roy, S.D., 1978. Fractionation of rare-earth elements in the Tuolumne intrusive series, Sierra Nevada Batholith, California. Geology 6, 239–242.
Gana, P., Tosdal, R.M., 1996. Geocronología U-Pb y K-Ar en intrusivos del Paleozoico y Mesozoico de la Cordillera de la Costa de la región de Valparaiso, Chile. Revista Geológica de Chile 23, 151–164.
Gans, C.R., Beck, S.L., Zandt, G., Gilbert, H., Alvarado, P., Anderson, M., Linkimer, L., 2011. Continental and oceanic crustal structure of the Pampean flat slab region, western Argentina, using receiver function analysis: new high-resolution results. Geophysical Journal International 186, 45–58.
Gatzoubaros, M., von Quadt, A., Gallhofer, D., Rey, R., 2014. Magmatic evolution of pre-ore volcanics and porphyry intrusives associated with the Altar Cu-porphyry prospect, Argentina. Journal of South American Earth Sciences 55, 58–82.
Ginibre, C., Wörner, G., Kronz, A., 2007. Crystal zoning as an archive for magma evolution. Elements 3, 261–266.
Halter, W.E., Bain, N., Becker, K., Heinrich, C.A., Landtwing, M., Von Quadt, A., Clark, A.H., Sasso, A.M., Bissig, T., Tosdal, R.M., 2004. From andesitic volcanism to the formation of a porphyry Cu-Au mineralizing magma chamber: the Farallon Negro volcanic complex, northwestern Argentina. Journal of Volcanology and Geothermal Research 136, 1–30.
Halter, W.E., Heinrich, C.A., Pettke, T., 2005. Magma evolution and the formation of porphyry Cu–Au ore fluids: evidence from silicate and sulfide melt inclusions. Mineralium Deposita 39 (8), 845–863.
Hattori, K.H., Keith, J.D., 2001. Contributions of mafic melt for porphyry deposits: evidence from Pinatubo and Bingham. Mineralium Deposita 36, 799–806.
Hattori, K., Sato, H., 1996. Magma evolution recorded in plagioclase zoning in 1991 Pinatubo eruption products. American Mineralogist 81 (7), 982–994.
Hedenquist, J.W., Lowenstern, J.B., 1994. The role of magmas in the formation of hydrothermal ore deposits. Nature 370, 519–527.
Hildreth, W., Moorbath, S., 1988. Crustal contributions to arc magmatism in the Andes of Central Chile. Contributions to Mineralogy and Petrology 98, 455–489.
Hunt, J.P., 1977. Porphyry copper deposits. Geological Society of London, Special Publications 7 (1), 98–98.
Jones, R.E., Kirstein, L.A., Kasemann, S.A., Dhuime, B., Elliott, T., Litvak, V.D., Alonso, R., Hinton, R., Facility, E.I.M., 2015. Geodynamic controls on the contamination of Cenozoic arc magmas in the southern Central Andes: insights from the O and Hf isotopic composition of zircon. Geochimica et Cosmochimica Acta 164, 386–402.
Jordan, T.E., Burns, W., Vega, R., Pángaro, F., Copeland, P., Kelley, S., Mpodozis, C., 2001. Extension and basin formation in the Southern Andes caused by increased convergence rate: a mid-Cenozoic trigger for the Andes. Tectonics 20, 308–324.
Kay, S.M., Abbruzzi, J.M., 1996. Magmatic evidence for Neogene lithospheric evolution of the central Andean "flat-slab" between 30°S and 32°S. Tectonophysics 259, 15–28.
Kay, S.M., Mpodozis, C., 2002. Magmatism as a probe to the Neogene shallowing of the Nazca plate beneath the modern Chilean flat-slab. Journal of South American Earth Sciences 15, 39–57.
Kay, S.M., Mpodozis, C., Ramos, V.A., Munizaga, F., 1991. Magma source variations for mid-late Tertiary magmatic rocks associated with a shallowing subduction zone and a thickening crust in the central Andes (28 to 33 S). In: Harmon, R.S., Rapela, C.W. (Eds.), Andean Magmatism and its Tectonic Setting, Geological Society of America Special Papers 265, pp. 113–137.
Kay, S.M., Mpodozis, C., Coira, B., 1999. Neogene magmatism, tectonism and mineral deposits of the central Andes (22°to 33°S Latitude). Society of Economic Geologists Special Publication 7, 27–59.
Kay, S.M., Godoy, E., Kurtz, A., 2005. Episodic arc migration, crustal thickening, subduction erosion, and magmatism in the south-central Andes. Geological Society of America Bulletin 117, 67–88.
Keith, J.D., Whitney, J.A., Hattori, K., Ballantyne, G.H., Christiansen, E.H., Barr, D.L., Cannan, T.M., Hooks, C.J., 1997. The role of magmatic sulfides and mafic alkaline magmas in the Bingham and Tintic mining districts, Utah. Journal of Petrology 38, 1679–1690.
Kelley, K.A., Cottrell, E., 2009. Water and the oxidation state of subduction zone magmas. Science 325 (5940), 605–607.
Klohn, C., 1960. Geología de la Cordillera de los Andes de Chile Central, Provs. de Santiago, Colchagua y Curicó. Instituto de Investigaciones Geológicas, Santiago, Boletín, p. 8.
Kurtz, A., Kay, S.M., Charrier, R., Farrar, E., 1997. Geochronology of Miocene plutons and Andean uplift history in the El Teniente region, central Chile (34–35 S). Revista Geológica de Chile 24, 75–90.
Lang, J.R., Titley, S.R., 1998. Isotopic and geochemical characteristics of Laramide magmatic systems in Arizona and implications for the genesis of porphyry copper deposits. Economic Geology 93 (2), 138–170.
Leake, B.E., Woolley, A.R., Arps, C.E., Birch, W.D., Gilbert, M.C., Grice, J.D., Linthout, K., 1997. Nomenclature of amphiboles: report of the subcommittee on amphiboles of the International Mineralogical Association Commission on new minerals and mineral names. Mineralogical Magazine 61 (2), 295–321.
LeHuray, A.P., Church, S.E., Koski, R.A., Bouse, R.M., 1988. Pb isotopes in sulfides from mid-ocean ridge hydrothermal sites. Geology 16 (4), 362–365.
Lickfold, V., Cooke, D.R., Crawford, A.J., Fanning, C.M., 2007. Shoshonitic magmatism and the formation of the Northparkes porphyry Cu–Au deposits, New South Wales. Australian Journal of Earth Sciences 54 (2–3), 417–444.
Liska Borba, M., Chemale Junior, F., Kawashita, K., Takehara, L., Babinski, M., Bruckman, M., 2016. The Bajo de la Alumbrera and Agua Rica Cu–Au (Mo) porphyry deposits of Argentina: genetic constraints on ore formation and sources based on isotope signatures. Ore Geology Reviews 75, 116–124.
Loucks, R.R., 2014. Distinctive composition of copper-ore-forming arc magmas. Australian Journal of Earth Sciences 61 (1), 5–16.
Macfarlane, A.W., 1999. Isotopic studies of northern Andean crustal evolution and ore metal sources. Society of Economic Geologists Special Publications 7, 195–217.
Maksaev, V., Munizaga, F., Zentilli, M., Charrier, R., 2009. Fission track thermochronology of Neogene plutons in the Principal Andean Cordillera of central Chile (33–35°S): implications for tectonic evolution and porphyry Cu-Mo mineralization. Andean Geology 36, 153–171.

Please cite this article in press as: Maydagán, L., et al., Petrogenesis of Quebrada de la Mina and Altar North porphyries (Cordillera of San Juan, Argentina): Crustal assimilation and metallogenic implications, Geoscience Frontiers (2016), http://dx.doi.org/10.1016/j.gsf.2016.11.011

Marek, J.M., 2014. Estimated mineral resources Altar and Quebrada de la Mina deposits, San Juan Province Argentina. Prepared by Independent Mining Consultants, Inc., for Stillwater Mining Company, Technical Report, 169 pp.
Martin, M.W., Clavero, J.R., Mpodozis, C.M., 1995. Estudio geológico regional de la franja del Indio. Cordillera de Coquimbo, Santiago, Chile. Informe registrado II–95–6, Servicio Nacional de Geología y Minería, Chile y Compañía Minera San José, 232 pp.
Martin, M.W., Clavero, J., Mpodozis, C., 1999. Late Paleozoic to Early Jurassic tectonic development of the high Andean Principal Cordillera, El Indio region, Chile (29–30 S). Journal of South American Earth Sciences 12 (1), 33–49.
Maughan, D., Keith, J., Christiansen, E., Pulsipher, T., Hattori, K., Evans, N., 2002. Contributions from mafic alkaline magmas to the Bingham porphyry Cu-Au-Mo deposit, Utah, USA. Mineralium Deposita 37, 14–37.
Maydagán, L., 2012. El Prospecto de Cu-(Au-Mo) Altar (31° 29′LS, 70°28′LO). San Juan: Unpublished Ph.D thesis. Universidad Nacional del Sur, Bahía Blanca, Argentina, 340 pp.
Maydagán, L., Franchini, M., Chiaradia, M., Pons, J., Impiccini, A., Toohey, J., Rey, R., 2011. Petrology of the Miocene igneous rocks in the Altar region, main Cordillera of San Juan, Argentina: a geodynamic model within the context of the Andean flat-slab segment and metallogenesis. Journal of South American Earth Sciences 32, 30–48.
Maydagán, L., Franchini, M., Chiaradia, M., Dilles, J., Rey, R., 2014. Intrusion history of the Altar porphyry Cu-(Mo-Au) deposit (Argentina): a complex magmatic-hydrothermal system with evidence of recharge processes. Economic Geology 109, 621–641.
Maydagán, L., Franchini, M., Rusk, B., Lentz, D.R., McFarlane, C., Impiccini, A., Rey, R., 2015. Porphyry to epithermal transition in the Altar Cu-(Au-Mo) deposit, Argentina, studied by Cathodoluminescence, LA-ICP-MS, and fluid inclusion analysis. Economic Geology 110 (4), 889–923.
Miller, J.S., Matzel, J.E., Miller, C.F., Burgess, S.D., Miller, R.B., 2007. Zircon growth and recycling during the assembly of large, composite arc plutons. Journal of Volcanology and Geothermal Research 167 (1), 282–299.
Mpodozis, C., Cornejo, P., 2012. Cenozoic tectonics and porphyry copper systems of the Chilean Andes. Society of Economic Geologists Special Publications 16, 329–360.
Mpodozis, C., Brockway, H., Marquardt, C., Perelló, J., 2009. Geocronología U-Pb y tectónica de la región Los Pelambres-Cerro Mercedario: implicancias para la evolución cenozoica de los Andes del centro de Chile y Argentina. In: Proc. Congreso Geológico Chileno XII, Santiago, Chile, pp. 1–4.
Muñoz, M., Fuentes, F., Vergara, M., Aguirre, L., Nyström, J.O., Féraud, G., Demant, A., 2006. Abanico East Formation: petrology and geochemistry of volcanic rocks behind the Cenozoic arc front in the Andean Cordillera, central Chile (33°50′S). Revista Geológica de Chile 33, 1,109–140.
Pearce, T.H., Kolisnik, A.M., 1990. Observations of plagioclase zoning using interference imaging. Earth Sciences Reviews 29 (1), 9–26.
Perelló, J., Sillitoe, R.H., Mpodozis, C., Brockway, H., Posso, H., 2012. Geologic setting and evolution of the porphyry copper-molybdenum and copper-gold deposits at Los Pelambres, central Chile. Society of Economic Geologists Special Publications 16, 79–104.
Reich, M., Parada, M.A., Palacios, C., Dietrich, A., Schultz, F., Lehmann, B., 2003. Adakite-like signature of Late Miocene intrusions at the Los Pelambres giant porphyry copper deposit in the Andes of central Chile: metallogenic implications. Mineralium Deposita 38, 876–885.
Richards, J.P., 2003. Tectono-magmatic precursors for porphyry Cu-(Mo-Au) deposit formation. Economic Geology 98, 1515–1533.
Richards, J.P., Boyce, A.J., Pringle, M.S., 2001. Geological evolution of the Escondida area, northern Chile: a model for spatial and temporal localization of porphyry Cu mineralization. Economic Geology 96, 271–305.
Ridolfi, F., Renzulli, A., 2012. Calcic amphiboles in calc-alkaline and alkaline magmas: thermobarometric and chemometric empirical equations valid up to 1,130° C and 2.2 Gpa. Contributions to Mineralogy and Petrology 163, 877–895.
Seedorff, E., Dilles, J., Proffett, J., Einaudi, M., 2005. Porphyry Deposits: Characteristics and Origin of Hypogene Features. Economic Geology 100th Anniversary, pp. 251–298.
Serrano, L., Vargas, R., Stambuk, V., Aguilar, C., Galeb, M., Holmgren, C., Contreras, A., Godoy, S., Vela, I., Skewes, A.M., Stern, C.R., 1996. The late Miocene to early Pliocene Río Blanco-Los Bronces copper deposit, central Chilean Andes. Society of Economic Geologists Special Publication 5, 119–129.
Sillitoe, R.H., 2010. Porphyry copper systems. Economic Geology 105 (1), 3–41.
Singer, B.S., Dungan, M., Layne, G.D., 1995. Textures and Sr, Ba, Mg, Fe, K, and Ti compositional profiles in volcanic plagioclase: clues to the dynamics of calcalkaline magma chambers. American Mineralogist 80, 776–798.
Singer, D.A., Berger, V.I., Moring, B.C., 2008. Porphyry Copper Deposits of the World. Database and grade and tonnage models, 2008: U.S. Geological Survey Open-File Report 2008, 1155, 45 pp.
Stern, C.R., 1991. Role of subduction erosion in the generation of Andean magmas. Geology 19, 78–81.
Stern, C.R., Skewes, M.A., Arévalo, A., 2010. Magmatic evolution of the giant El Teniente Cu-Mo deposit, Central Chile. Journal of Petrology 52, 1591–1617.
Sun, W., Huang, R.F., Li, H., Hu, Y.B., Zhang, C.C., Sun, S.J., Ling, M.X., 2015. Porphyry deposits and oxidized magmas. Ore Geology Reviews 65, 97–131.
Tafti, R., Mortensen, J.K., Lang, J.R., Rebagliati, M., Oliver, J.L., 2009. Jurassic U-Pb and Re-Os ages for the newly discovered Xietongmen Cu-Au porphyry district, Tibet, PRC: implications for metallogenic epochs in the southern Gangdese belt. Economic Geology 104 (1), 127–136.
Tepley, F.J., Davidson, J.P., Tilling, R.I., Arth, J.G., 2000. Magma mixing, recharge and eruption histories recorded in plagioclase phenocrysts from El Chichon Volcano, Mexico. Journal of Petrology 41 (9), 1397–1411.
Tilton, G.R., 1979. Isotopic studies of Cenozoic Andean calc-alkaline rocks. Carnegie Institution Washington Year 78, 298–303.
Tilton, G.R., Pollak, R.J., Clark, A.H., Robertson, R.C., 1981. Isotopic composition of Pb in central Andean ore deposits. Geological Society of America Memoirs 154, 791–816.
Titley, S.R., 1991. Correspondence of ores of silver and gold with basement terranes in the American southwest. Mineralium Deposita 26 (1), 66–71.
Tosdal, R.M., 1995. Metal source differences in Cenozoic porphyry Cu-Mo-Au deposits in the central Chilean Andes between 26° and 28°: an influence on the size of porphyry deposits? In: Clark, A.H., Hodgson, C.J., Mason, R. (Eds.), Proceedings of the Second Giant Ore Deposits Workshop, Giant Ore Deposits-II; Controls on the Scale of Orogenic Magmatic-hydrothrmal Mineralization. Queen's University, Kingston, Ontario, Canada, pp. 124–138.
Tosdal, R.M., Munizaga, F., 2003. Lead sources in Mesozoic and Cenozoic Andean ore deposits, north-central Chile (30–34 S). Mineralium Deposita 38, 234–250.
Tosdal, R.M., Wooden, J.L., Bouse, R.M., 1999. Pb isotopes, ore deposits, and metallogenic terranes. In: Lambert, D.D., Brown, P.E. (Eds.), Application of Radiogenic Isotopes to Ore Deposit Research and Exploration. Society of Economic Geologists, Littleton, pp. 1–25.
Wallace, P., Carmichael, I.S., 1992. Sulfur in basaltic magmas. Geochimica et Cosmochimica Acta 56 (5), 1863–1874.
Wilkinson, J.J., 2013. Triggers for the formation of porphyry ore deposits in magmatic arcs. Nature Geosciences 6 (11), 917–925.
Williamson, B.J., Herrington, R.J., Morris, A., 2016. Porphyry copper enrichment linked to excess aluminium in plagioclase. Nature Geoscience. http://dx.doi.org/10.1038/NGEO2651.
Winchester, J.A., Floyd, P.A., 1977. Geochemical discrimination of different magma series and their differentiation products using immobile elements. Chemical Geology 20, 325–343.
Winocur, D., Ramos, V., 2008. Geología y Estructura del sector norte de la Alta Cordillera de la provincia de San Juan. In: Proc. Congreso Geológico Argentino No. 17, pp. 166–167 (in Spanish with English abstract).
Winocur, D.A., Litvak, V.D., Ramos, V.A., 2014. Magmatic and tectonic evolution of the Oligocene Valle del Cura basin, main Andes of Argentina and Chile: evidence for generalized extension. Geological Society of London,Special Publications 399, 109–130.
Wu, C., Chen, H., Hollings, P., Xu, D., Liang, P., Han, J., Xiao, B., Cai, K., Liu, Z., Qi, Y., 2015. Magmatic sequences in the Halasu Cu Belt, NW China: trigger for the Paleozoic porphyry Cu mineralization in the Chinese Altay–East Junggar. Ore Geology Reviews 71, 373–404.
Yáñez, G., Ranero, G., von Huene, R., Diaz, J., 2001. Magnetic anomaly interpretation across a segment of the southern central Andes (32°–34°S): implications on the role of the Juan Fernández Ridge in the tectonic evolution of the margin during the upper tertiary. Journal Geophysical Research 106, 6325–6345.
Zartman, R.E., 1974. Lead isotopic provinces in the Cordillera of the western United States and their geologic significance. Economic Geology 69 (6), 792–805.
Zindler, A., Hart, S., 1986. Chemical geodynamics. Annual Review of Earth and Planetary Sciences 14, 493–571.
Zwahlen, C., Cioldi, S., Wagner, T., Rey, R., Heinrich, C., 2014. The porphyry Cu–(Mo–Au) deposit at Altar (Argentina): tracing gold distribution by vein mapping and LA–ICP–MS mineral analysis. Economic Geology 109, 1341–1358.

Please cite this article in press as: Maydagán, L., et al., Petrogenesis of Quebrada de la Mina and Altar North porphyries (Cordillera of San Juan, Argentina): Crustal assimilation and metallogenic implications, Geoscience Frontiers (2016), http://dx.doi.org/10.1016/j.gsf.2016.11.011